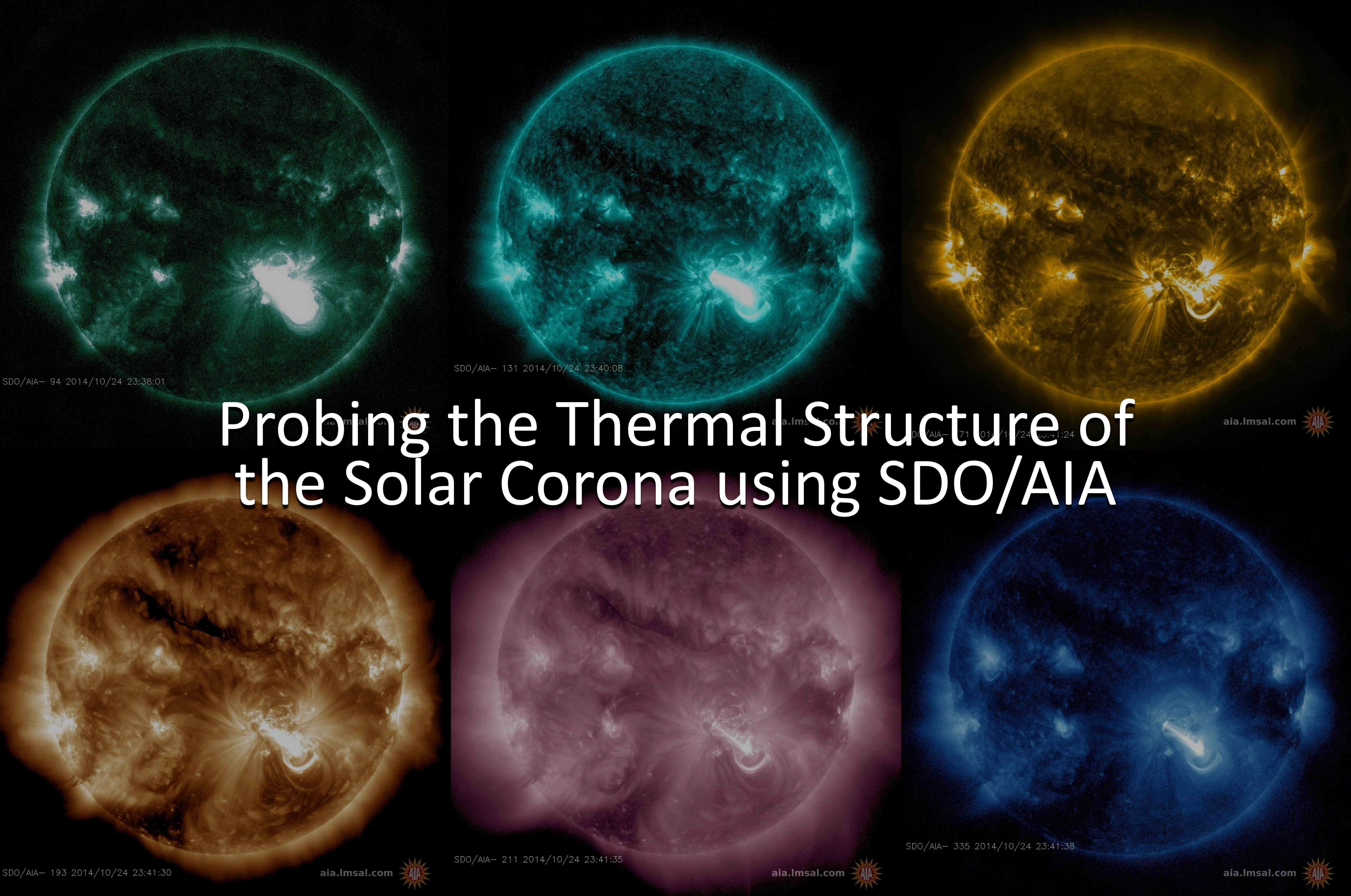

Probing the Thermal Structure of the Solar Corona using SDO/AIA

Mark Cheung, Lockheed Martin Solar & Astrophysics Laboratory
Visiting Associate Professor @ National Astronomical Observatory of Japan

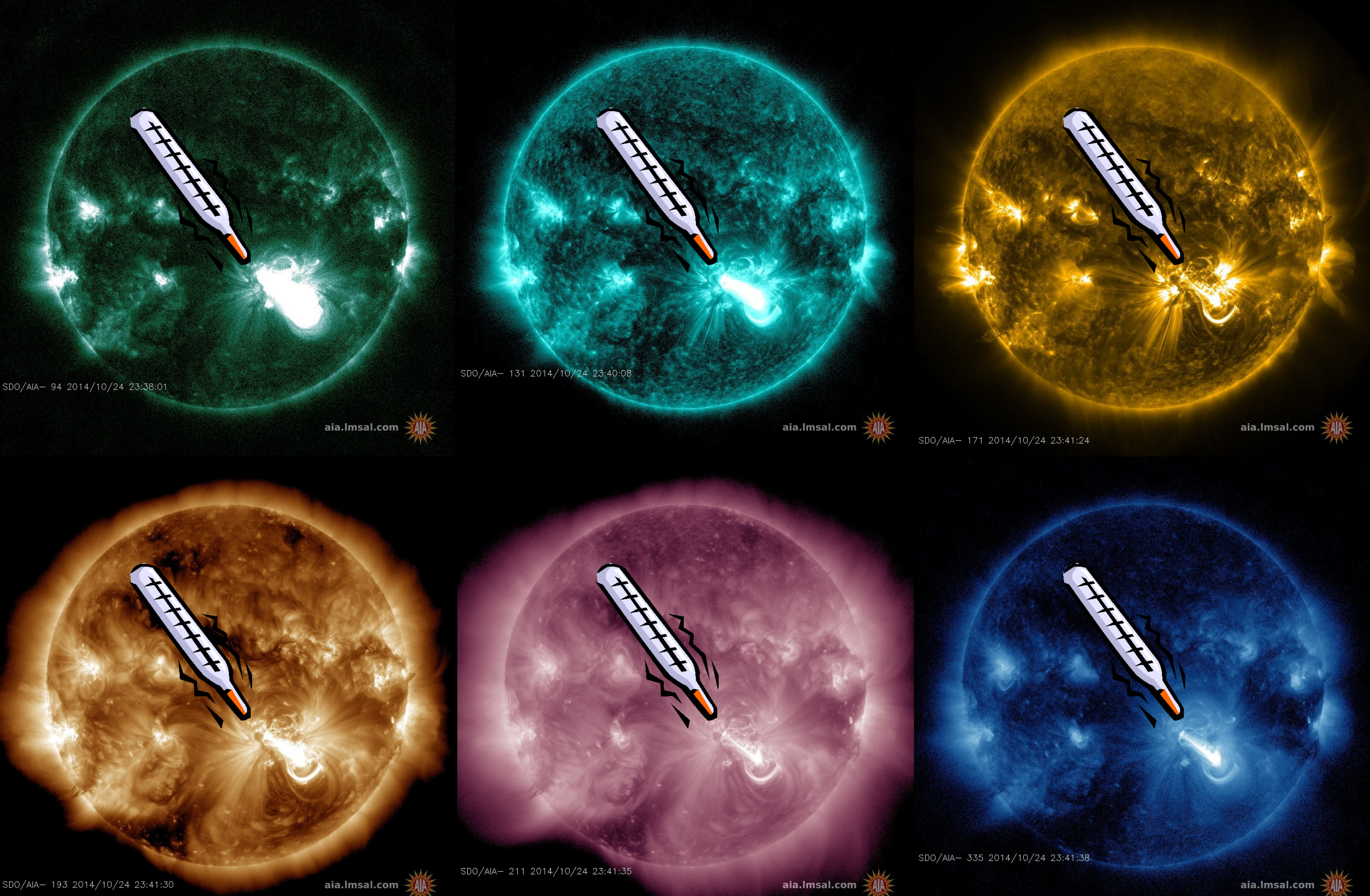

AIA is not just Another Imaging Assembly. It was designed with the promise of thermal diagnostics.

Statement of the Problem

The Atmospheric Imaging Assembly (AIA, Lemen et al. 2012; Boerner et al. 2012) instrument onboard NASA's Solar Dynamics Observatory (SDO, Pesnell et al. 2012) is a suite of four normal-incidence reflecting telescopes that image the Sun in seven EUV channels, two UV channels and one visible wavelength channel.

The aim of this and many other studies is to extract thermal information about the Sun's optically thin corona using the EUV observations. The calibrated (i.e. dark-subtracted, flat-fielded and exposure time normalized) count rate y_i in the i-th EUV channel is related to the thermal distribution of coronal plasma by:

$$y_i = \int_0^\infty K_i(T)\ \mathrm{DEM}(T) dT,$$

where $K_i(T)$ is the temperature response function (see next slide):

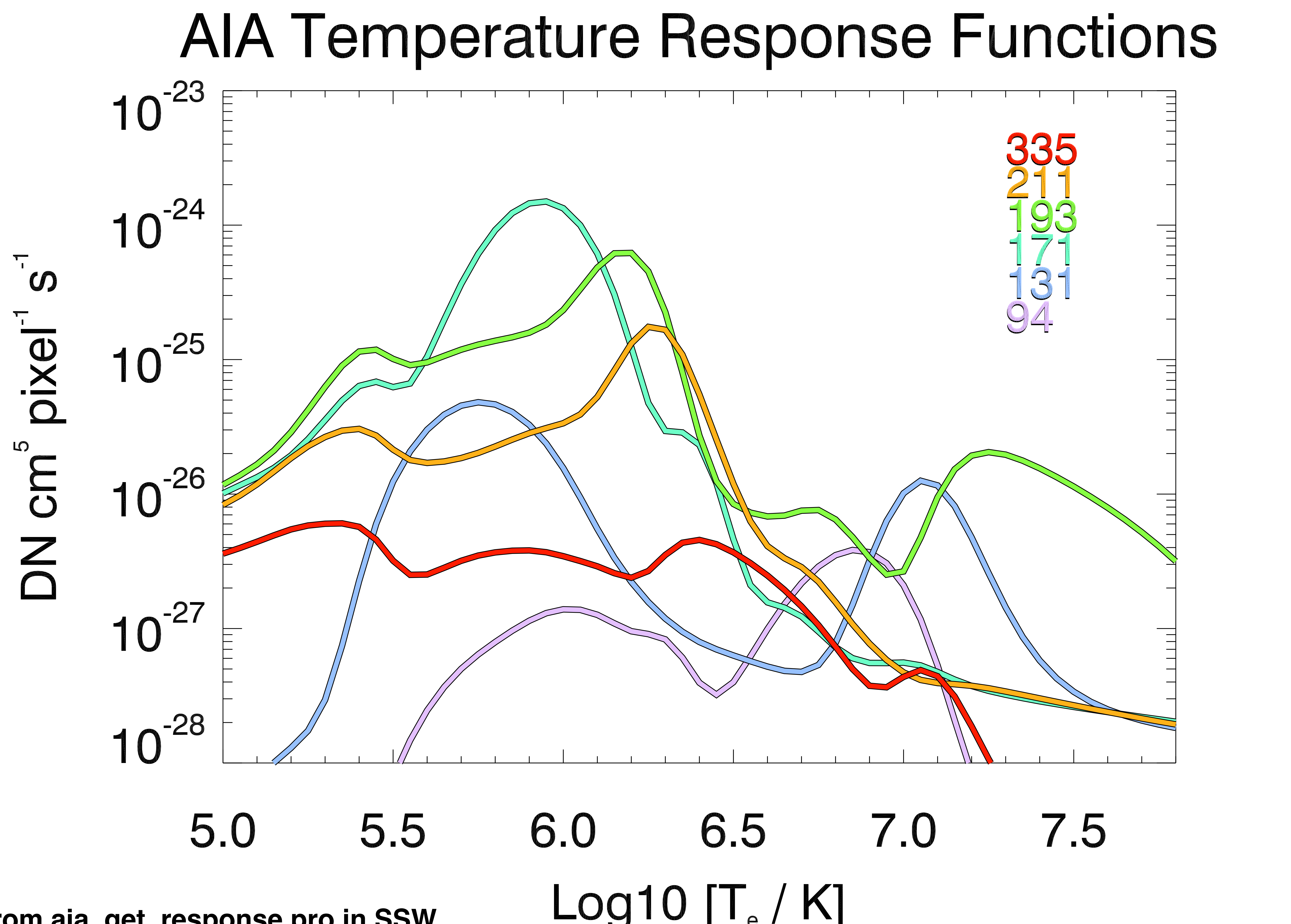

From aia_get_response.pro in SSW

Table 1. Predicted AIA count rates.

	Ion	λ	$T_{\rm p}^{\rm a}$	Fraction of total emission			
		Å	K	CH	QS	AR	FL
94 Å	Mg VIII	94.07	5.9	0.03	-	-	-
	Fe XX	93.78	7.0	-	-	-	0.10
	Fe XVIII	93.93	6.85	-	-	0.74	0.85
	Fe X	94.01	6.05	0.63	0.72	0.05	-
	Fe VIII	93.47	5.6	0.04	-	-	-
	Fe VIII	93.62	5.6	0.05	-	-	-
	Cont.			0.11	0.12	0.17	-
131 Å	O VI	129.87	5.45	0.04	0.05	-	-
	Fe XXIII	132.91	7.15	-	-	-	0.07
	Fe XXI	128.75	7.05	-	-	-	0.83
	Fe VIII	130.94	5.6	0.30	0.25	0.09	-
	Fe VIII	131.24	5.6	0.39	0.33	0.13	-
	Cont.			0.11	0.20	0.54	0.04
171 Å	Ni XIV	171.37	6.35	-	-	0.04	-
	Fe X	174.53	6.05	-	0.03	-	-
	Fe IX	171.07	5.85	0.95	0.92	0.80	0.54
	Cont.			-	-	-	0.23
193 Å	O V	192.90	5.35	0.03	-	-	-
	Ca XVII	192.85	6.75	-	-	-	0.08
	Ca XIV	193.87	6.55	-	-	0.04	-
	Fe XXIV	192.03	7.25	-	-	-	0.81
	Fe XII	195.12	6.2	0.08	0.18	0.17	-
	Fe XII	193.51	6.2	0.09	0.19	0.17	-
	Fe XII	192.39	6.2	0.04	0.09	0.08	-
	Fe XI	188.23	6.15	0.09	0.10	0.04	-
	Fe XI	192.83	6.15	0.05	0.06	-	-
	Fe XI	188.30	6.15	0.04	0.04	-	-
	Fe X	190.04	6.05	0.06	0.04	-	-
	Fe IX	189.94	5.85	0.06	-	-	-
	Fe IX	188.50	5.85	0.07	-	-	-
	Cont.			-	-	0.05	0.04
211 Å	Cr IX	210.61	5.95	0.07	-	-	-
	Ca XVI	208.60	6.7	-	-	-	0.09
	Fe XVII	204.67	6.6	-	-	-	0.07
	Fe XIV	211.32	6.3	-	0.13	0.39	0.12
	Fe XIII	202.04	6.25	-	0.05	-	-
	Fe XIII	203.83	6.25	-	-	0.07	-
	Fe XIII	209.62	6.25	-	0.05	0.05	-
	Fe XI	209.78	6.15	0.11	0.12	-	-
	Fe X	207.45	6.05	0.05	0.03	-	-
	Ni XI	207.92	6.1	0.03	-	-	-
	Cont.			0.08	0.04	0.07	0.41
304 Å	He II	303.786	4.7	0.33	0.32	0.27	0.29
	He II	303.781	4.7	0.66	0.65	0.54	0.58
	Ca XVIII	302.19	6.85	-	-	-	0.05
	Si XI	303.33	6.2	-	-	0.11	-
	Cont.			-	-	-	-
335 Å	Al X	332.79	6.1	0.05	0.11	-	-
	Mg VIII	335.23	5.9	0.11	0.06	-	-
	Mg VIII	338.98	5.9	0.11	0.06	-	-
	Si IX	341.95	6.05	0.03	0.03	-	-
	Si VIII	319.84	5.95	0.04	-	-	-
	Fe XVI	335.41	6.45	-	-	0.86	0.81
	Fe XIV	334.18	6.3	-	0.04	0.04	-
	Fe X	184.54	6.05	0.13	0.15	-	-
	Cont.			0.08	0.05	-	0.06

From O'Dwyer et al. 2010

Statement of the Problem

and $$\mathrm{DEM}(T)dT = \int_0^\infty n_e^2(T)dz,$$

where DEM(T) is the differential emission measure (in units of cm^{-5} K^{-1}) of plasma along the line-of-sight. $n_e(T)$ is the electron number density of plasma at temperature T. The challenge is to solve for DEM(T) given a set of EUV measurements **y**.

Let the temperature range be divided into n neighboring bins, so that:

$$y_i = \sum_{j=1}^{n} \int_{T_j}^{T_j+\Delta T_j} K_i(T)\mathrm{DEM}(T)dT,$$

where the j-th temperature bin has range $T \in [T_j, T_j+\Delta T_j)$. Assuming that $K_i(T)$ is piecewise constant in each temperature bin, we have:

$$y_i = \sum_{j=1}^{n} K_{ij}\mathrm{EM}_j, \text{where } \mathrm{EM}_j = \int_{T_j}^{T_j+\Delta T_j} \mathrm{DEM}(T)dT.$$

Statement of the Problem: y = Kx

$$y_i = \sum_{j=1}^{n} K_{ij} \mathrm{EM}_j, \text{ where } \mathrm{EM}_j = \int_{T_j}^{T_j + \Delta T_j} \mathrm{DEM}(T) dT.$$

The above is a matrix equation of the form **y** = K**x,** where

- K is an m x n response matrix*, with each row corresponding to the temperature response function of one AIA channel
- **y** is an m-tuple corresponding of AIA count (rates), and
- **x** is an n-tuple with components EM_j.

The He II line in the 304 Å channel is not well-modeled by CHIANTI (Warren, 2005, ApJ 157, 147) so it is usually not used for DEM analysis. So m = 6 for AIA. Usually we want more than 6 temperature bins. **For m < n, the matrix equation y = Kx represents an underdetermined system.**

*Matrix elements depends on basis functions used for computing the integral

Usual Approach: χ-squared Minimization

<u>**Function to minimize:**</u> **$| y - Kx |^2$ or $|(y - Kx)/\sigma|^2$**

Basically, minimize difference between observed and predicted counts. The benefits of a least-squares approach is that it leads to Euler-Lagrange equations that can be used to seek (global or local) minima.

For an overdetermined system, we know no single model will fit all the data. So χ-squared minimization is ideal. However, **for underdetermined systems such an approach can be subject to the perils of overfitting.**

Usual way to get around this:

Parameterization: e.g. Guennou et al (2012a,b), xrt_dem_iterative2.pro (M. Weber in SSW, see also Cheng et al 2012)

Regularization: e.g. Hannah & Kontar (2012), Plowman et al. (2013)

Cheung et al. 2015: The Sparse Solution

We address the inverse problem using an approach different than chi-squared minimization. The set of solutions satisfying the underdetermined matrix equation **y** = K**x** lies in an affine subspace of $\mathbf{R}^n$. We pick the solution $\mathbf{x}^{\#}$ within this subspace such that:

$$\text{minimize} \sum_{j}^{n} \mathrm{x}_j \text{ subject to } \mathcal{K}\vec{x} = \vec{y},\ \vec{x} \geq 0.$$

The linear program above finds a solution that minimizes the L1-norm of the solution vector (c.f. Candes 2006). This is not chi-squared minimization.

If K is the response function sampled by Dirac Delta functions at specific temperatures, this is equivalent to minimizing the total EM. If other basis functions are used, there is no simple corresponding physical interpretation.

The Sparse Solution

We are unaware of physical principles pertaining to coronal plasma that motivate the optimization problem posed above. However, this choice has some important benefits:

1) It does not overfit (consistent with the principle of parsimony, i.e. Ockham's Razor).
2) It ensures positivity of the solution (if solutions exist).
3) It is an L1-norm minimization problem, so we can use standard techniques from compressed sensing (c.f. Candes & Tao 2006).

   BTW the L1-norm of a vector $x = \mathbf{\Sigma}\ |x_i|$

4) Speed: $O(10^4)$ solutions / sec with single IDL thread.

See Asensio Ramos & De La Cruz Rodriguez (2015) for application of related techniques to 2D coupled Stokes inversion.

Handling noise

In practice, measurement uncertainties imply that the equality **y** = K**x** may not be satisfied. So our method solves the followed modified linear program:

$$\text{minimize} \sum_j^n \mathrm{x}_j \text{ subject to } \mathcal{K}\vec{x} \leq \vec{y} + \vec{\eta},$$
$$\vec{x} \geq 0,\ \mathcal{K}\vec{x} \geq \max(\vec{y} - \vec{\eta}, 0).$$

The vector **η** is a measure of the uncertainty in the count rate and provides tolerance for the predicted counts (K**x)** to deviate from the observed values (**y**). To enforce positive counts the lower bound is set to max(**y**-**η**, 0).

χ-squared minimization

Sparse inversion

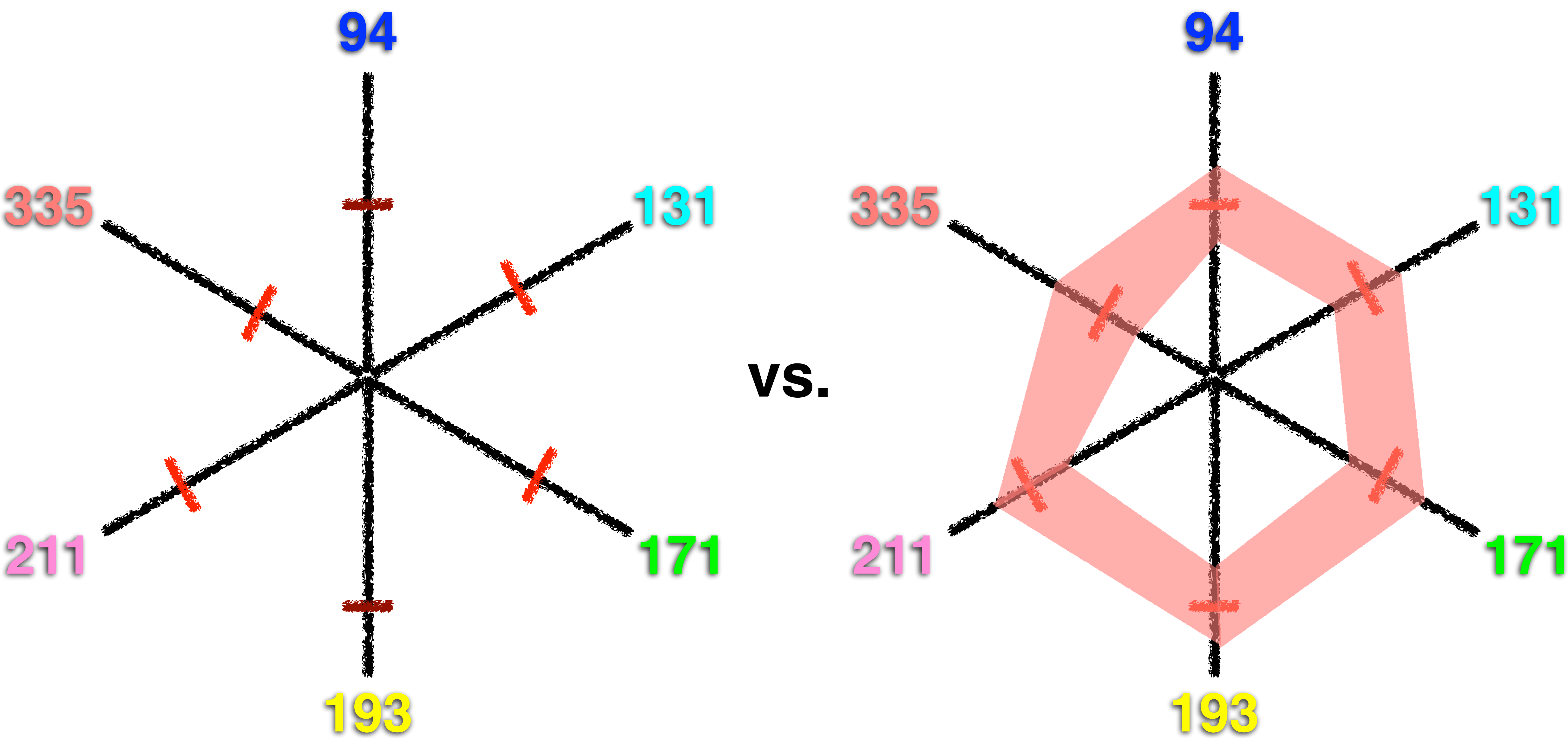

Crossmarks are observed counts

Subspace of allowed solutions in our method

Basis Functions for DEM

Let $i = 1, 2, ..., m$ denote the index over a set of wavelength band channels and/or line spectra. Let the DEM function be written in terms of a set of positive semidefinite basis functions $\{b_j(\log T) \geq 0 \mid k = 1, 2, ..., l\}$, viz.

$$\mathrm{DEM}(\log T) = \sum_{k=1}^{l} b_k(\log T) x_k, \tag{A1}$$

with quadrature coefficients $x_k \geq 0$. Approximating the integrals in equation (1) as sums in $\log T$ space, we have

$$y_i = \sum_{j=1}^{n} \sum_{k=1}^{l} K_{ij} B_{jk} x_k \Delta \log T, \tag{A2}$$

where $j = 1, 2, ..., n$ is the index over temperature bins, $K_{ij} = K_i(\log T_j)$ and $B_{jk} = b_k(\log T_j)$. The response matrix $\mathbf{K} = (K_{ij})$ has dimensions $m \times n$. The basis matrix $\mathbf{B} = (B_{jk})$ has dimensions $n \times l$, with the k-th column vector corresponding to the k-th basis function $b_k(\log T_j)$. Defining the *dictionary matrix* $\boxed{\mathbf{D} = \mathbf{KB}}$, the set of integral equations (1) can be written in matrix form:

In practice we solve this ➜

$$\boxed{\vec{y} = \mathbf{D}\vec{x},} \tag{A3}$$

where the sought-after solution vector $\vec{x}$ is an l-tuple with components $x_k \Delta \log T$ $(k = 1, 2, ..., l)$. When the number of basis functions exceeds the number of image channels (i.e. $l > m$), the linear system Eq. (A3) is underdetermined.

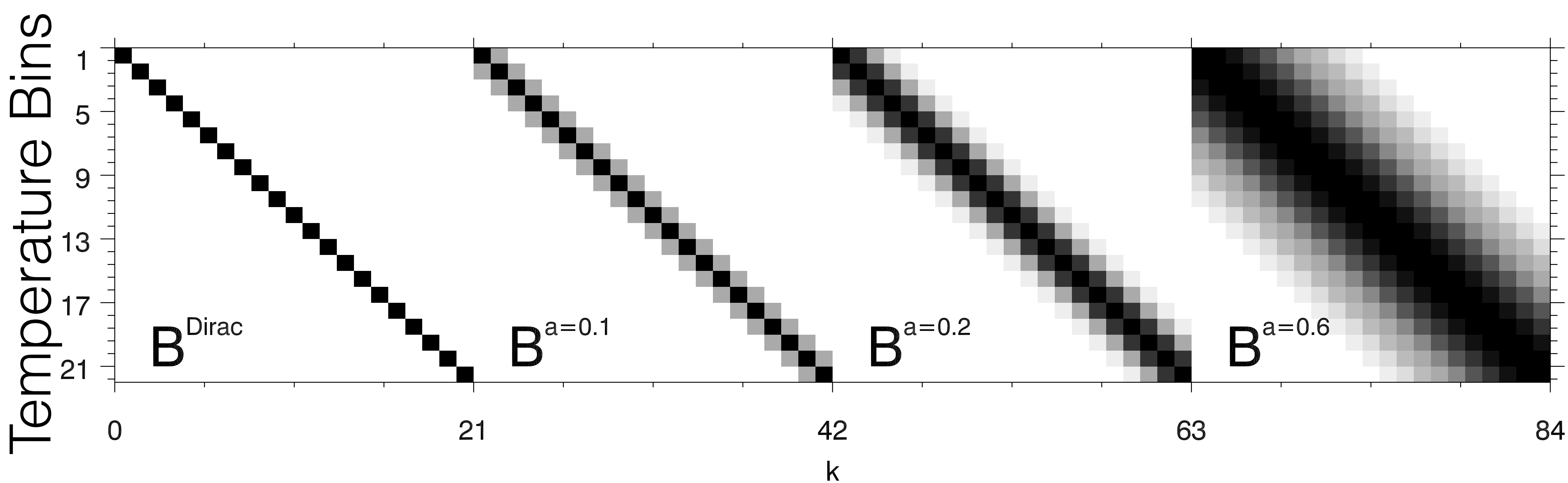

Validation Exercise 1: Gaussian DEMs

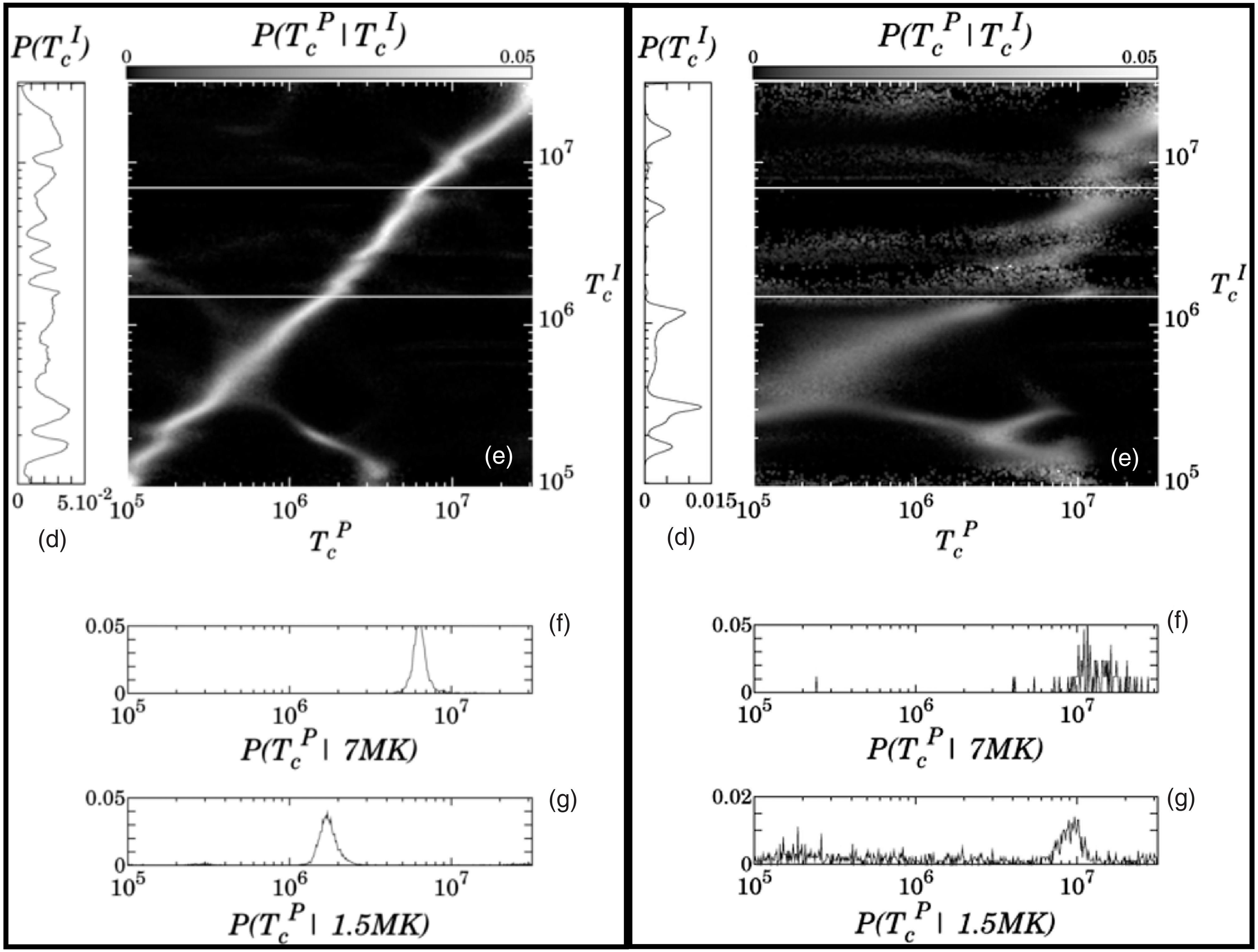

Guennou et al (2012) reported that when the input gaussian is moderately wide (0.3 log Te, right panel), AIA 6-channel inversions yield spurious temperatures.

Test DEMs: $\xi(T, T_c, \sigma) = \frac{\mathrm{EM}_0}{\sigma\sqrt{2\pi}} \exp\left[-\frac{(\log T - \log T_c)^2}{2\sigma^2}\right]$ $\mathrm{EM}_0 = 10^{29}\ \mathrm{cm}^2$

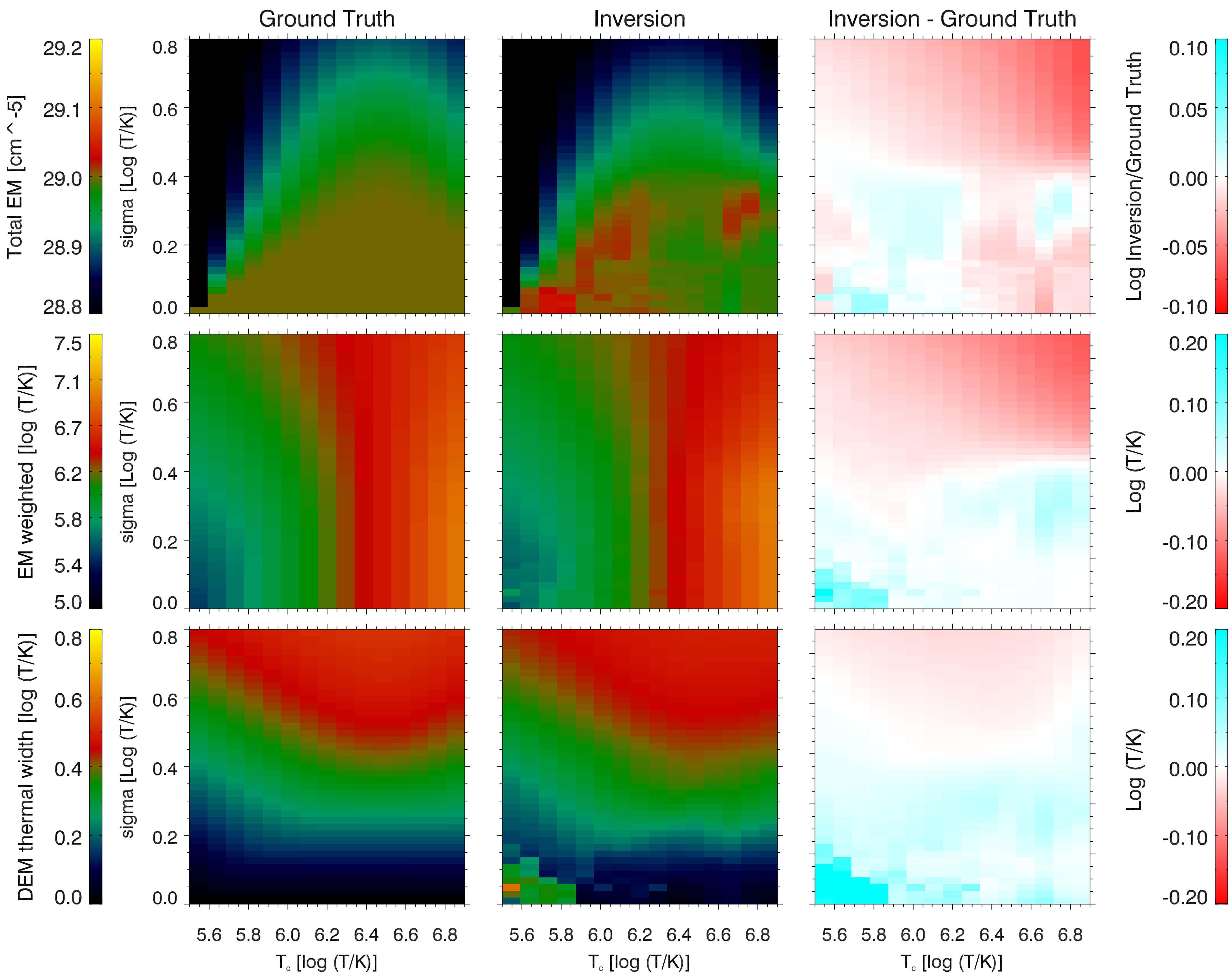

Validation Exercise 2: Quasi-steady loops in a NLFFF model of AR 11158

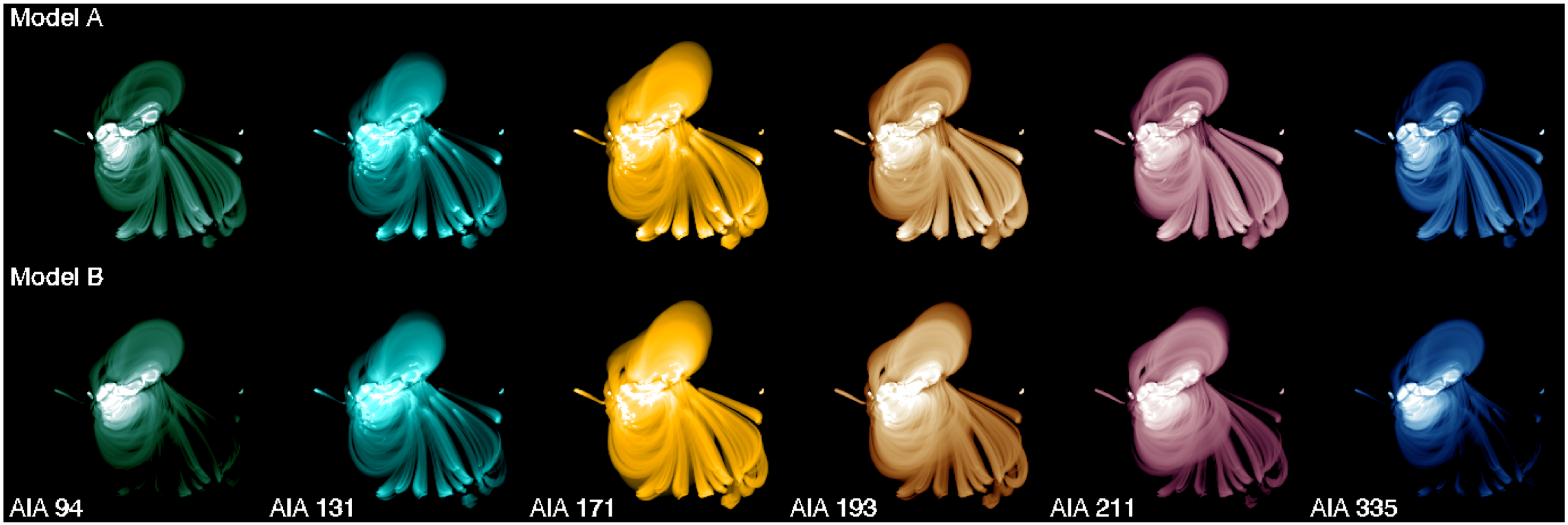

Fig. 5.— Synthetic AIA images (log-scaled) for the two thermal models (top and bottom rows) of NOAA AR 11158.

Magnetic Model: Quasi-Grad-Rubin Non-linear force-free Field reconstruction of AR 11158.
Thermal Model: Quasi-steady loops with different heating functions.

AR 11158 Model A

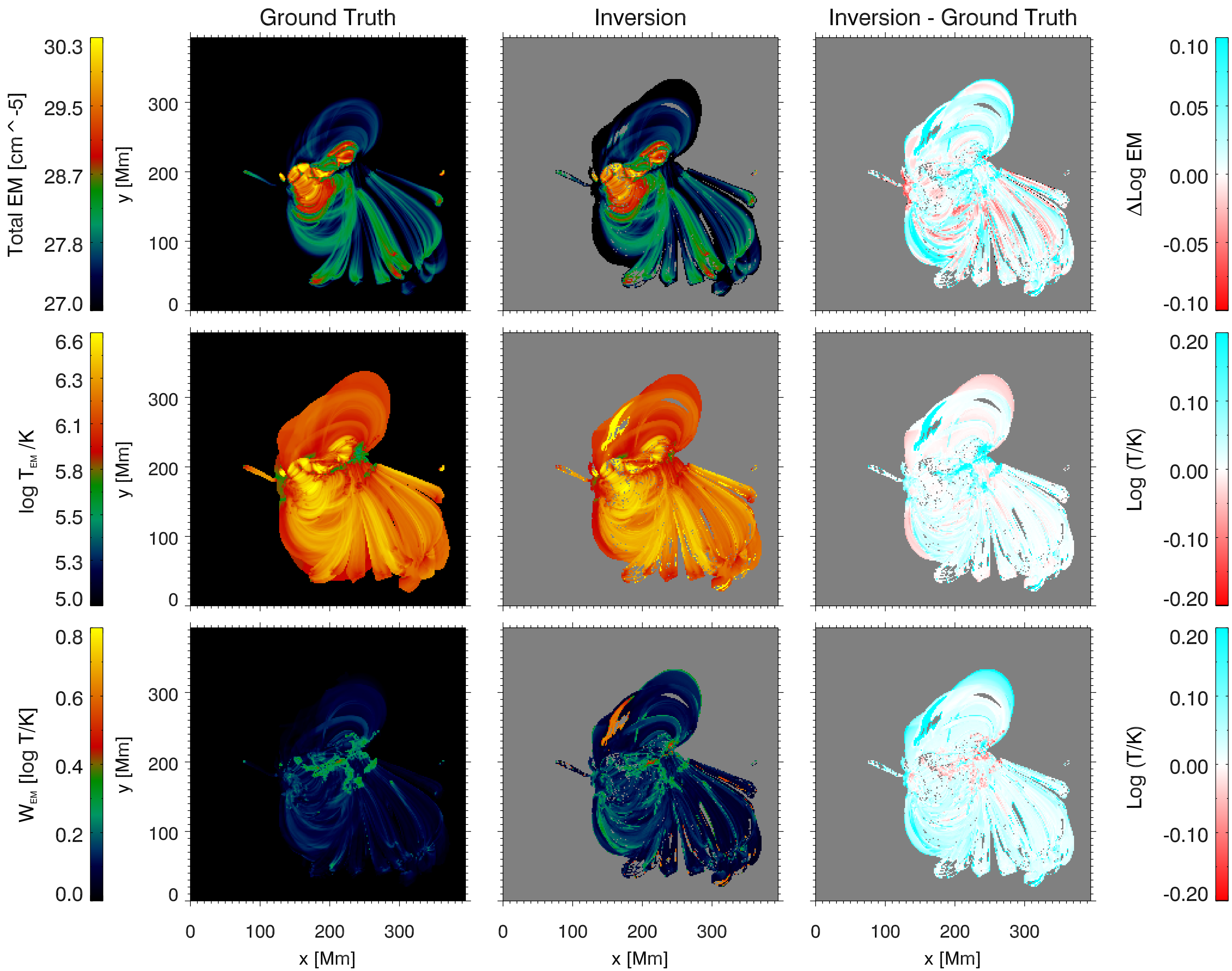

AR 11158 Model B

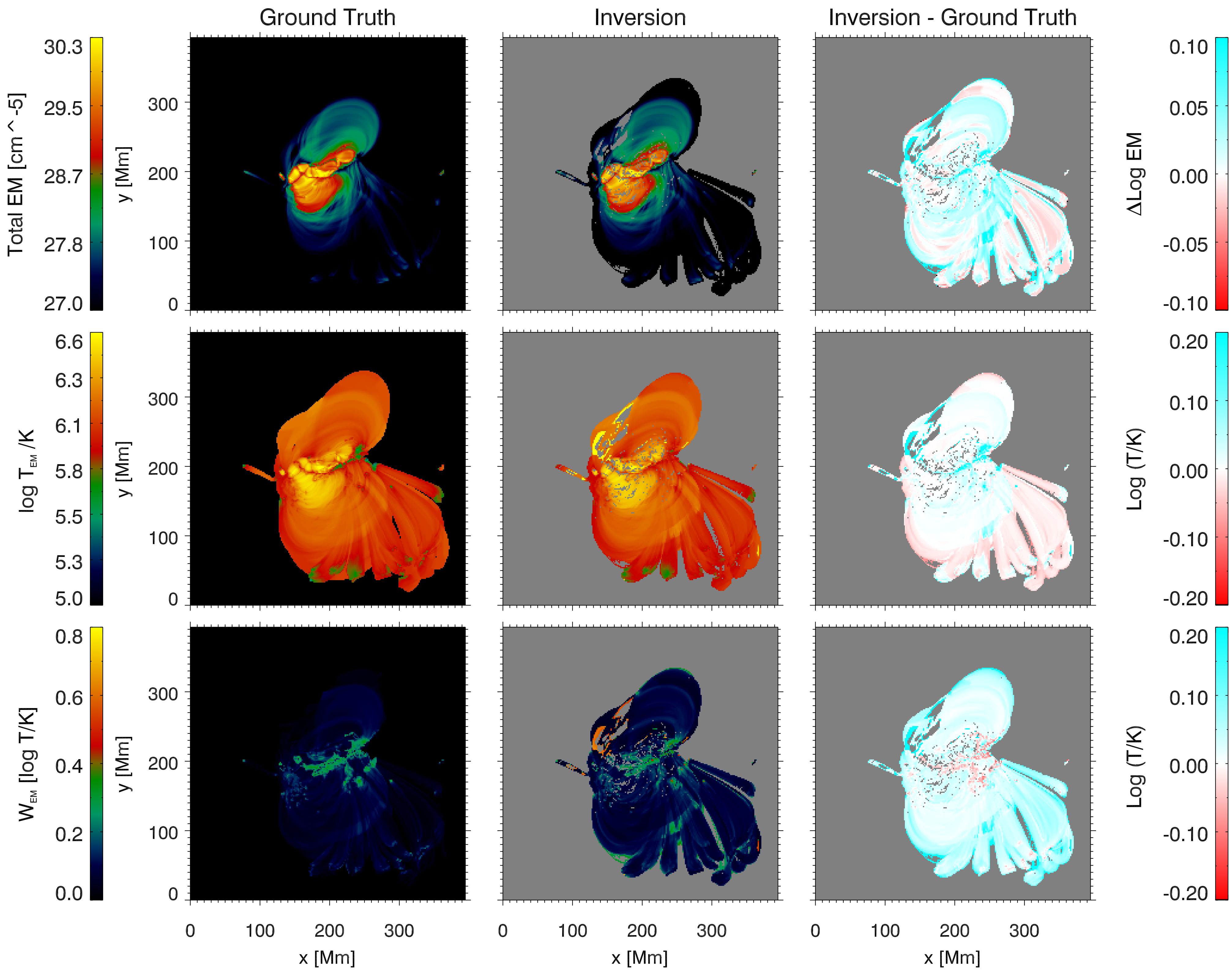

Validation Exercise 3: MHD Model

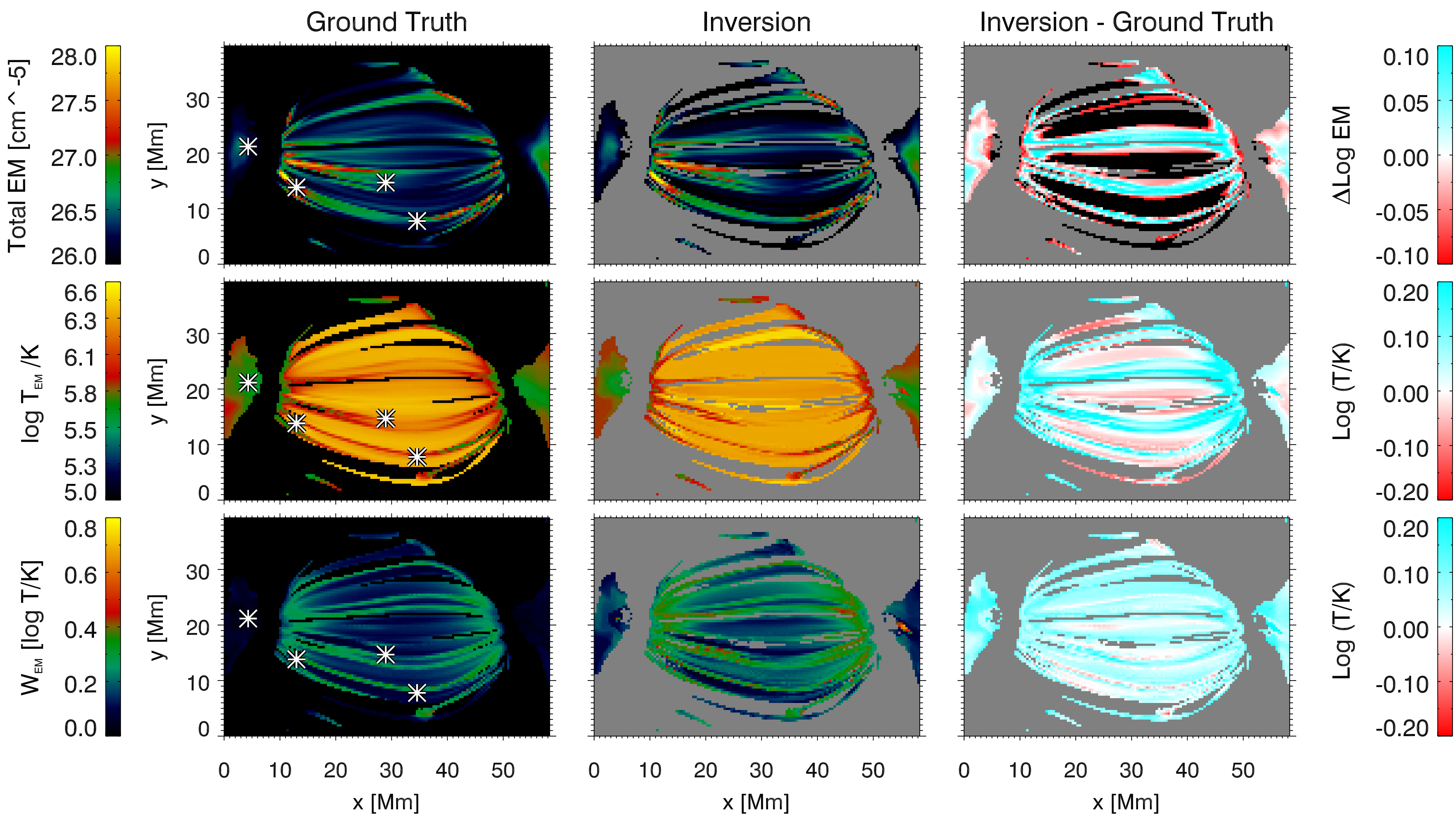

MHD model of AR formation (with thermal conduction) by Chen et al. (2014A&A...564A..12C, 2015NatPh..11..492C)

Validation Exercise 3: MHD Model

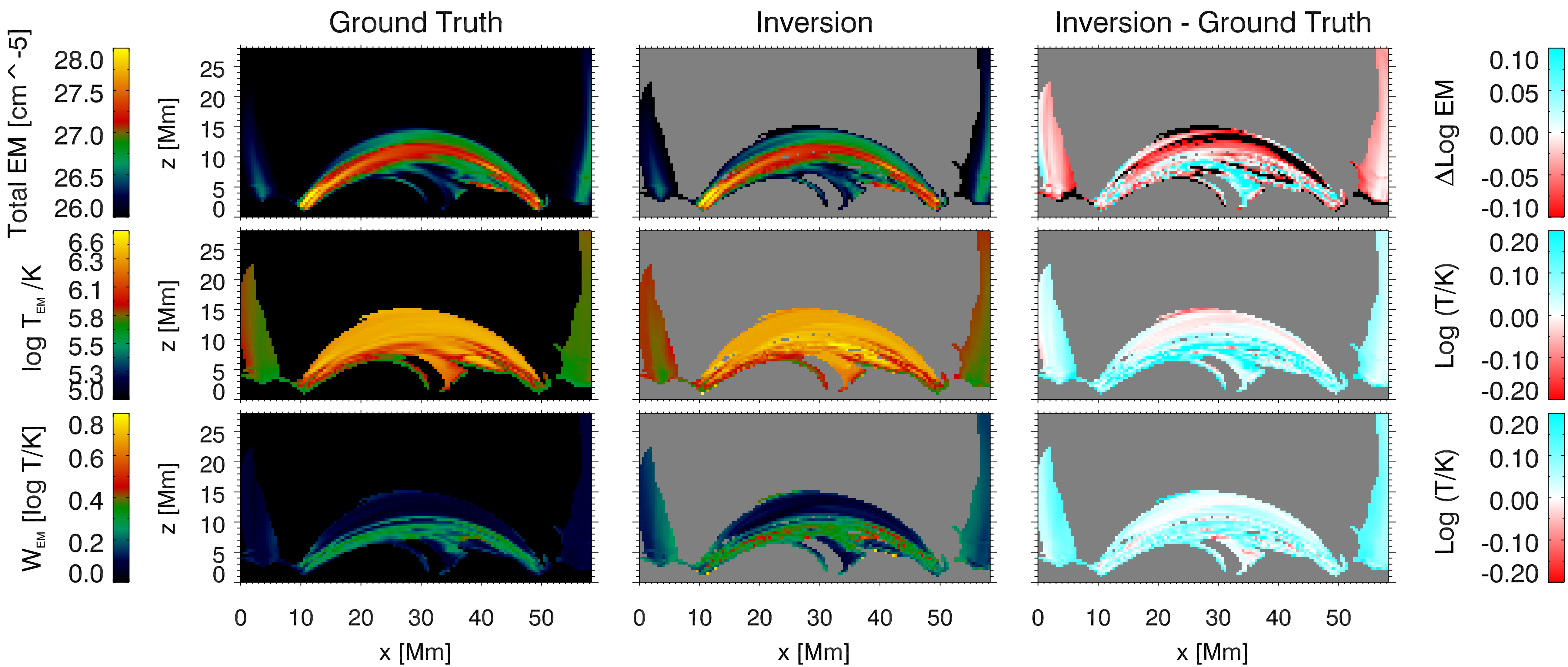

MHD model of AR formation (with thermal conduction) by Chen et al. (2014A&A…564A..12C, 2015NatPh..11..492C)

Validation Exercise 4*: AIA-XRT Cross-Comparison

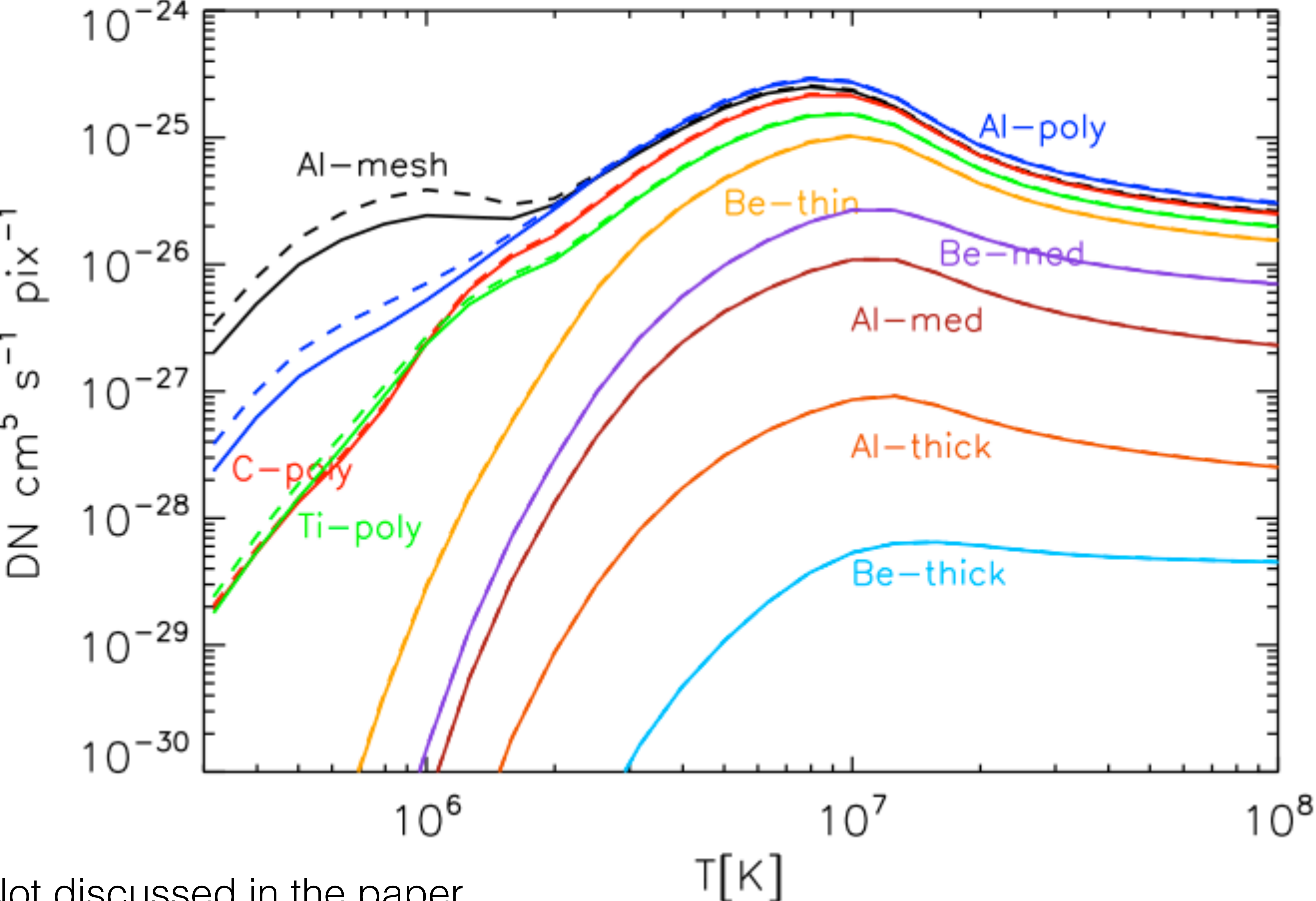

*Not discussed in the paper

AIA-XRT Cross-Comparison Analysis Procedure

1. Load and prep an XRT image.
2. Cutout AIA 94, 131, 171, 193, 211 & 335 level 1.5 data for XRT FOV as indicated by FITS keywords.
    1. DEM inversion (sun_coronal_ext.abund, chianti.ioneq).
    2. Sample DEMs onto XRT plate scale.
    3. Synthesize XRT image by folding response function against AIA DEM.
3. Use tr_get_disp to align actual and synthetic XRT images.
4. Compare (following slides).

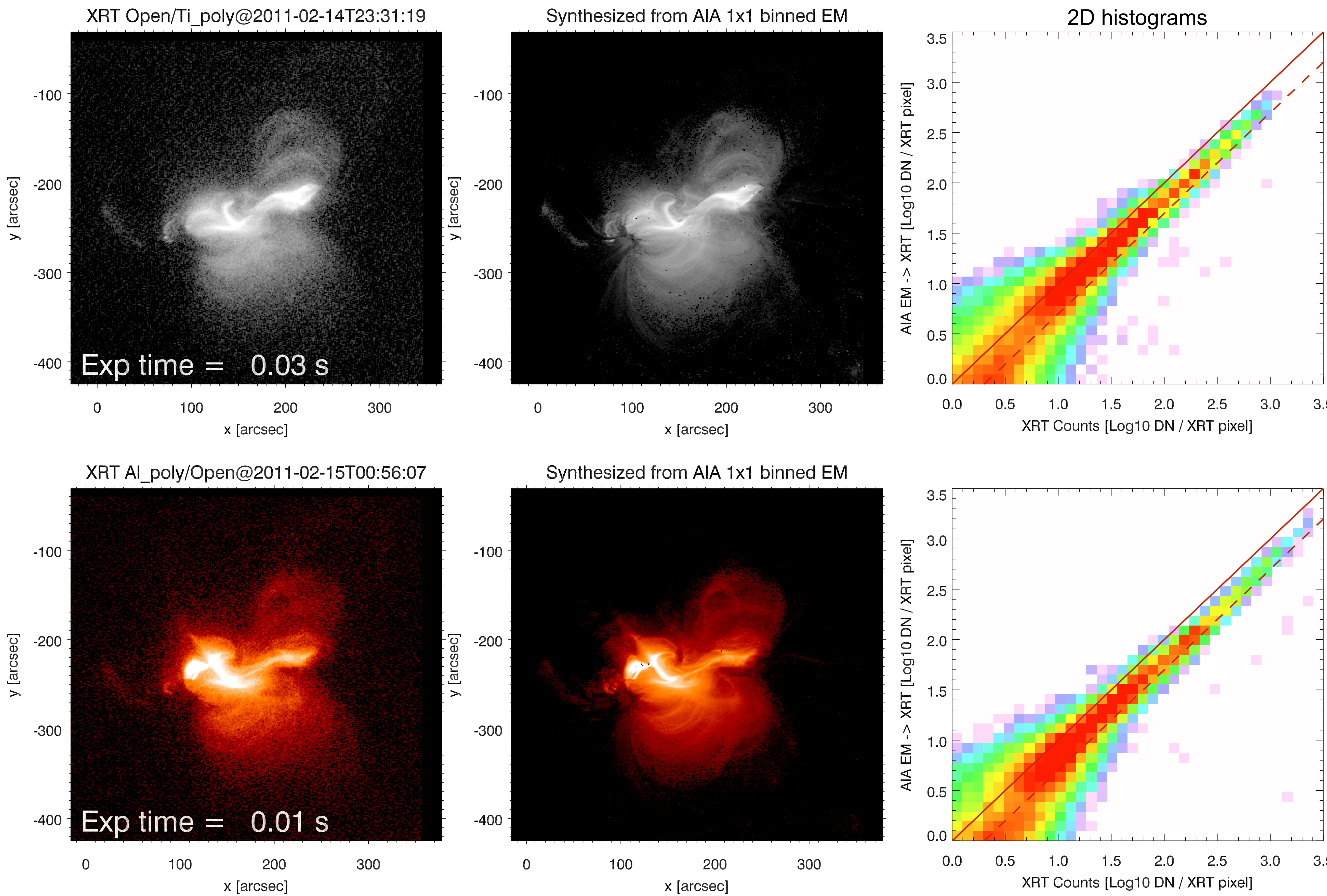
XRT Open/Ti_poly@2011-02-14T23:31:19
Exp time = 0.03 s
Synthesized from AIA 1x1 binned EM
2D histograms
AIA EM -> XRT [Log10 DN / XRT pixel]
XRT Counts [Log10 DN / XRT pixel]
XRT Al_poly/Open@2011-02-15T00:56:07
Exp time = 0.01 s
Synthesized from AIA 1x1 binned EM
AIA EM -> XRT [Log10 DN / XRT pixel]
XRT Counts [Log10 DN / XRT pixel]
x [arcsec]
y [arcsec]

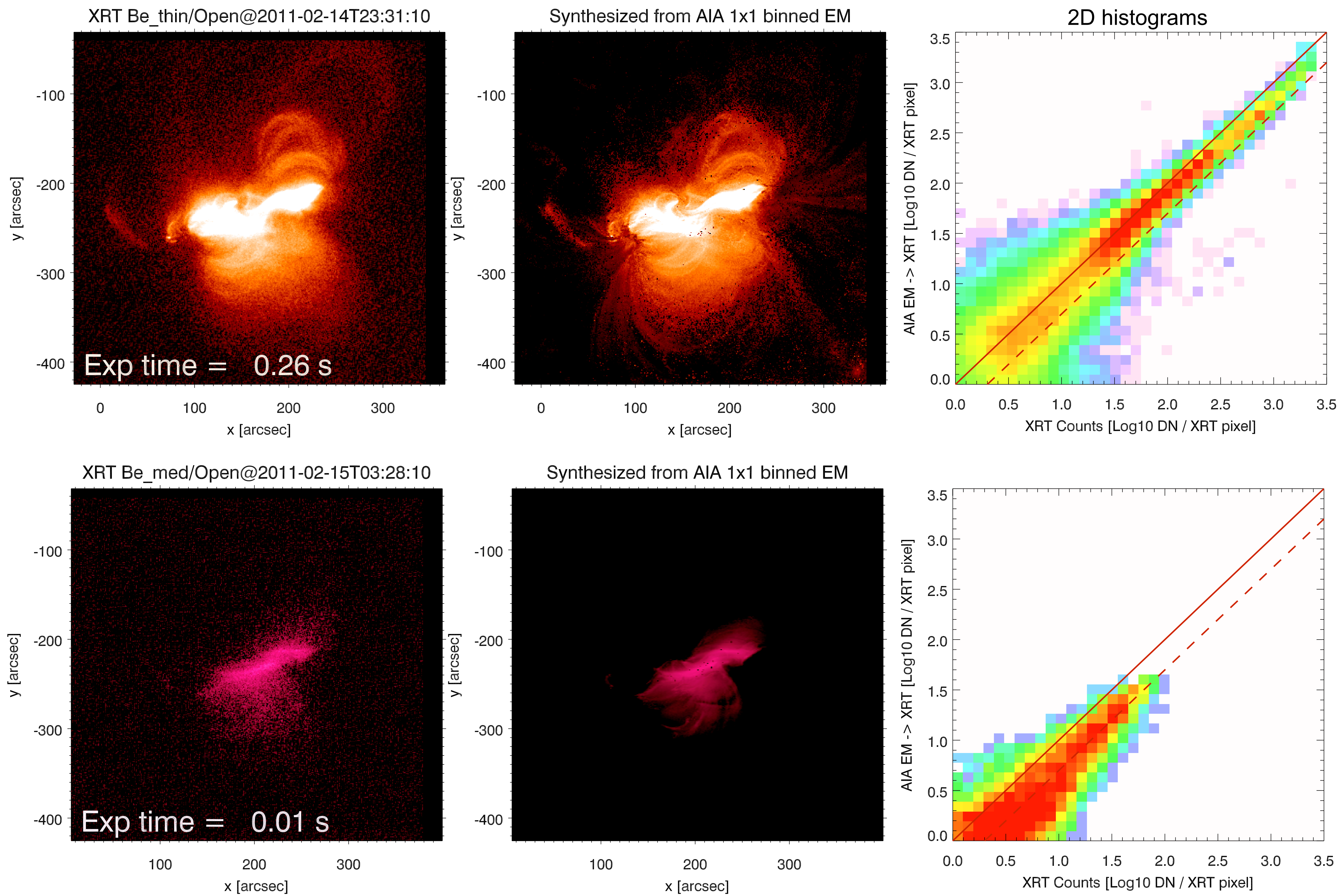

XRT Be_thin/Open@2011-02-14T23:31:10
Exp time = 0.26 s
Synthesized from AIA 1x1 binned EM
2D histograms
XRT Counts [Log10 DN / XRT pixel]
AIA EM -> XRT [Log10 DN / XRT pixel]
XRT Be_med/Open@2011-02-15T03:28:10
Exp time = 0.01 s
Synthesized from AIA 1x1 binned EM
x [arcsec]
y [arcsec]

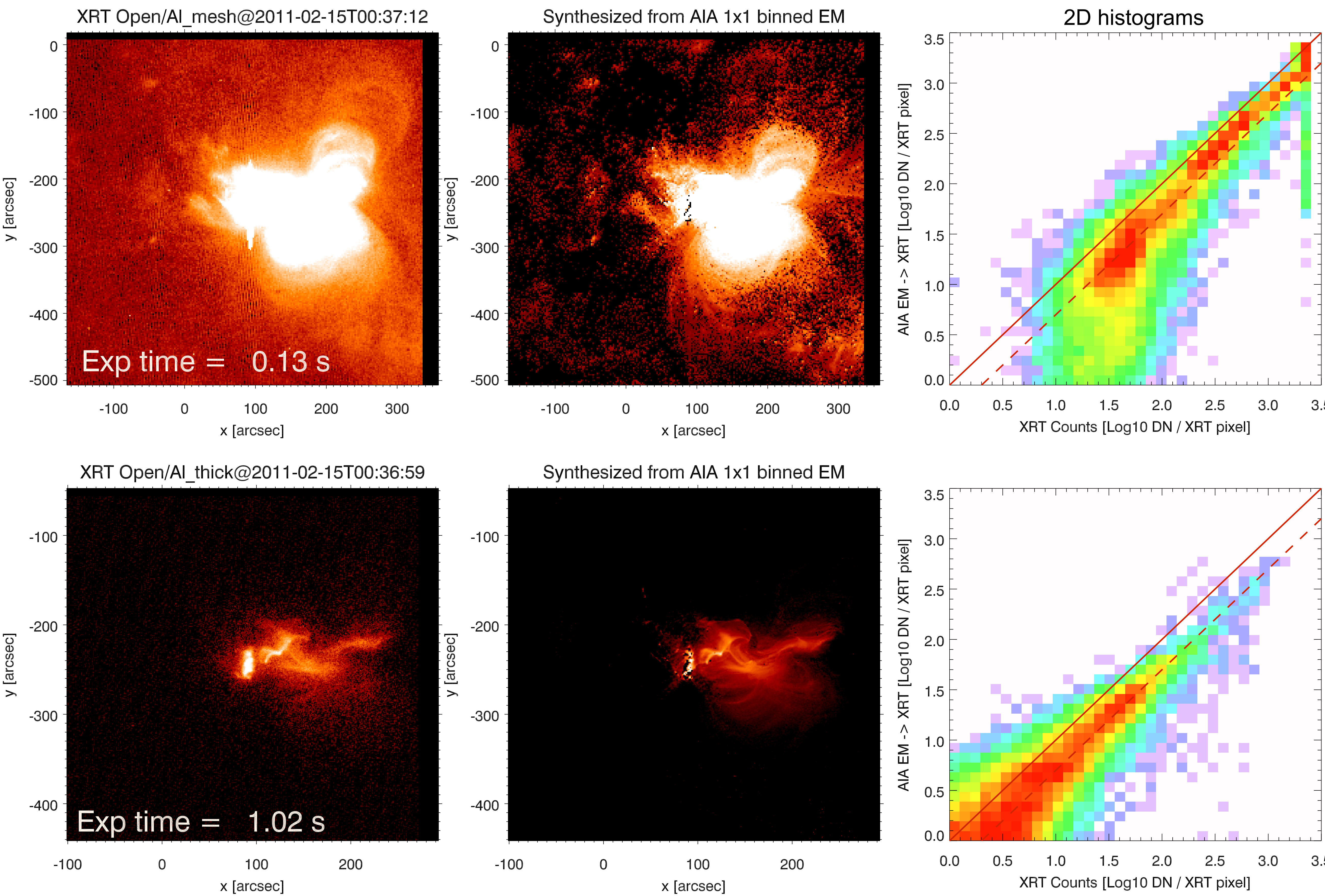

XRT Open/Al_mesh@2011-02-15T00:37:12
Exp time = 0.13 s
Synthesized from AIA 1x1 binned EM
2D histograms
y [arcsec]
x [arcsec]
AIA EM -> XRT [Log10 DN / XRT pixel]
XRT Counts [Log10 DN / XRT pixel]
XRT Open/Al_thick@2011-02-15T00:36:59
Exp time = 1.02 s
Synthesized from AIA 1x1 binned EM

Synthetic XRT Images

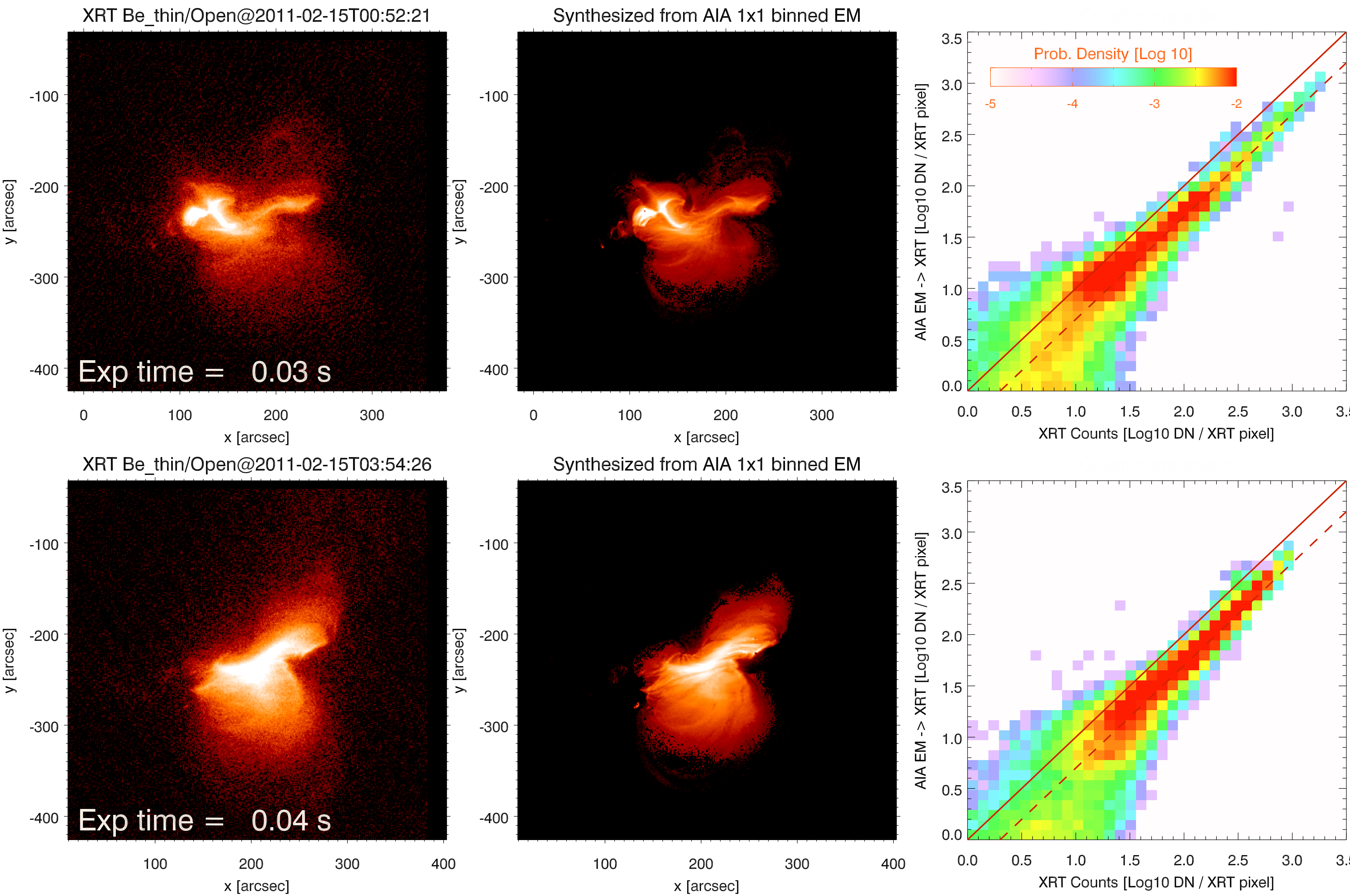

Validation Exercise 4: AIA-XRT Cross-Comparison

- Synthetic XRT images from DEMs derived using only AIA Reproduces morphology, but counts are too low compared to XRT by ~ 30 - 40%.

- Is this good enough?

- Is the discrepancy between synthetic and real XRT images due to limitations of the inversion, or due to uncertainties of the absolute calibration of both instruments?

Log-normal DEMs: AIA 6 channels only

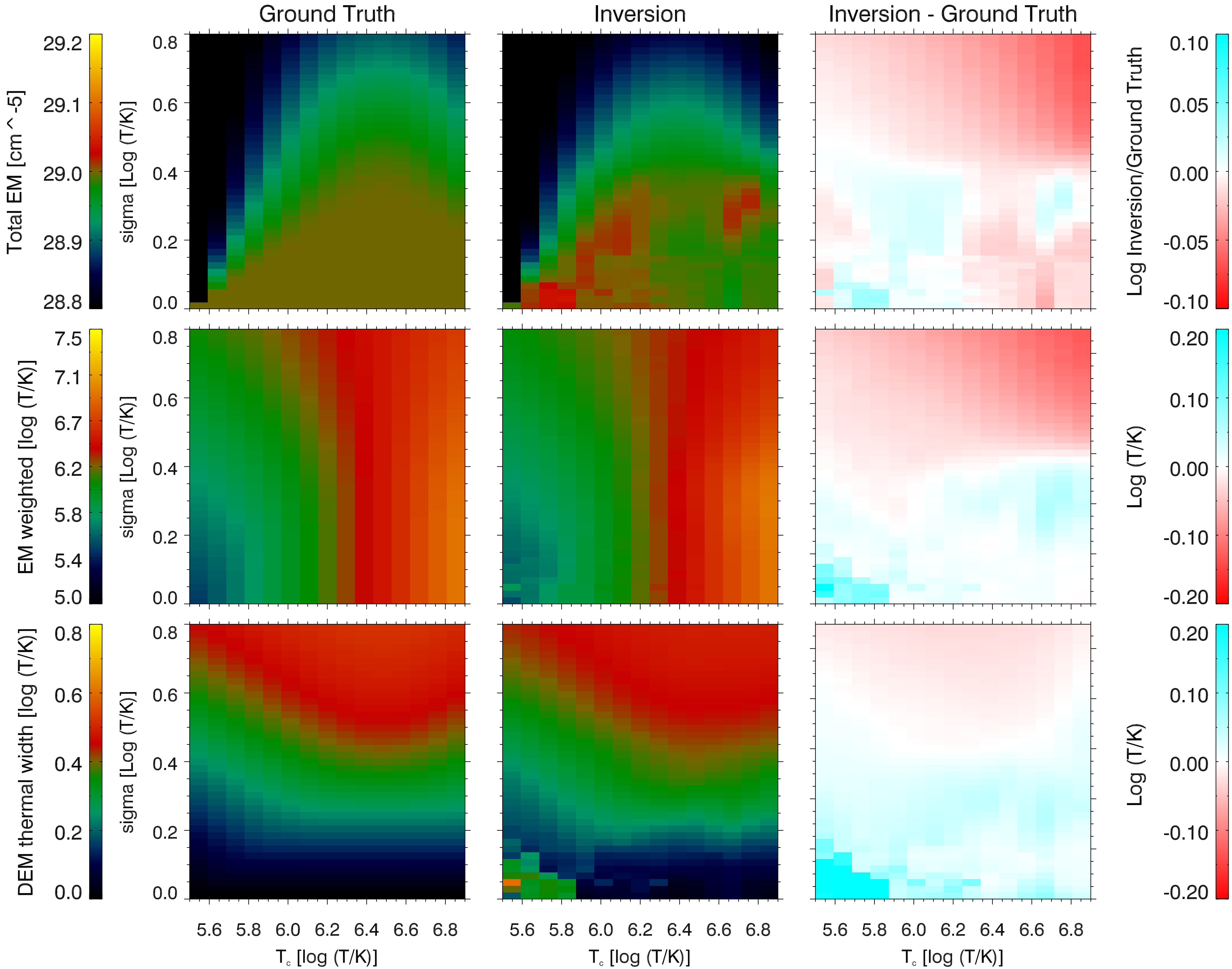

Log-normal DEMs: AIA 6 channels + XRT Be-thin

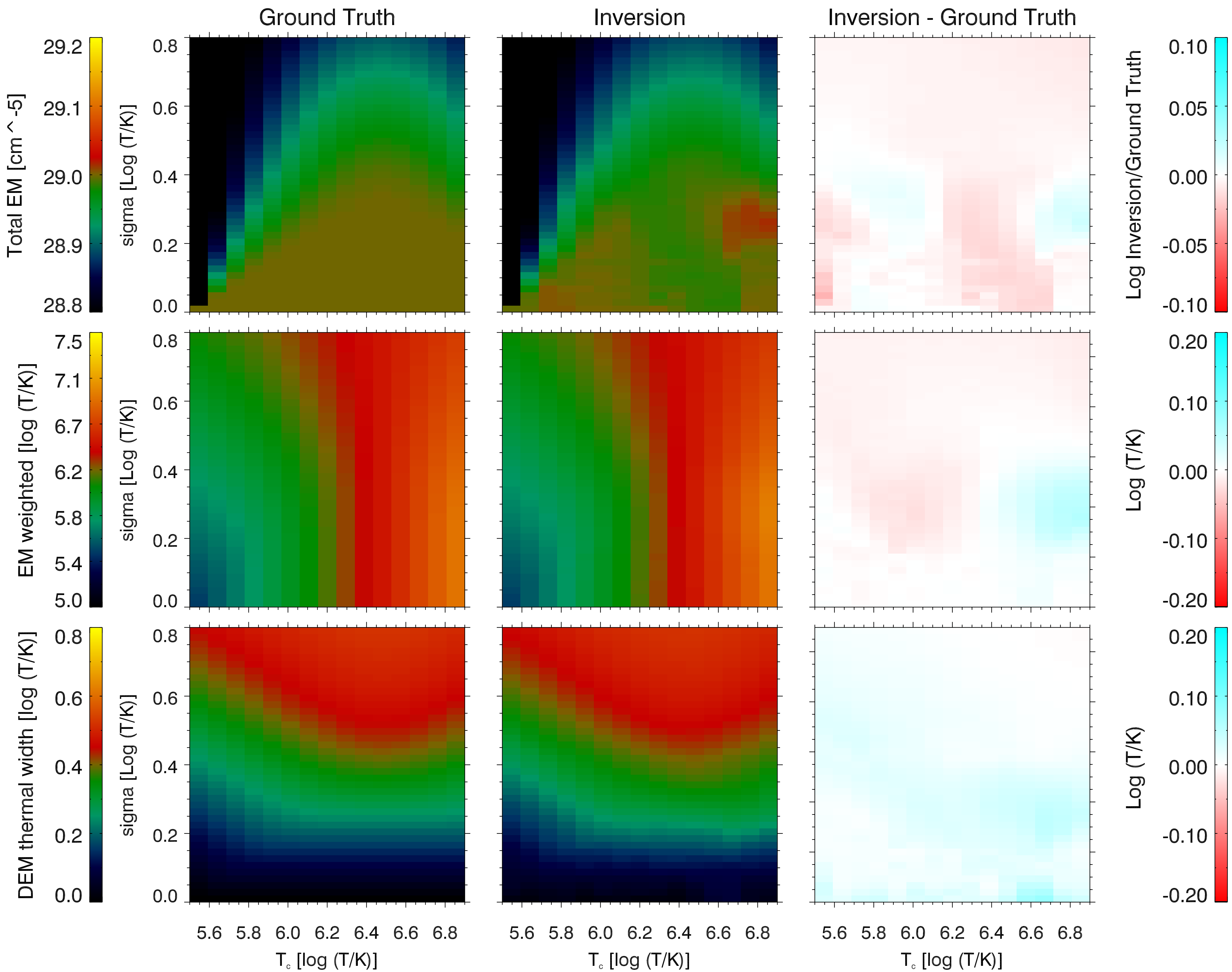

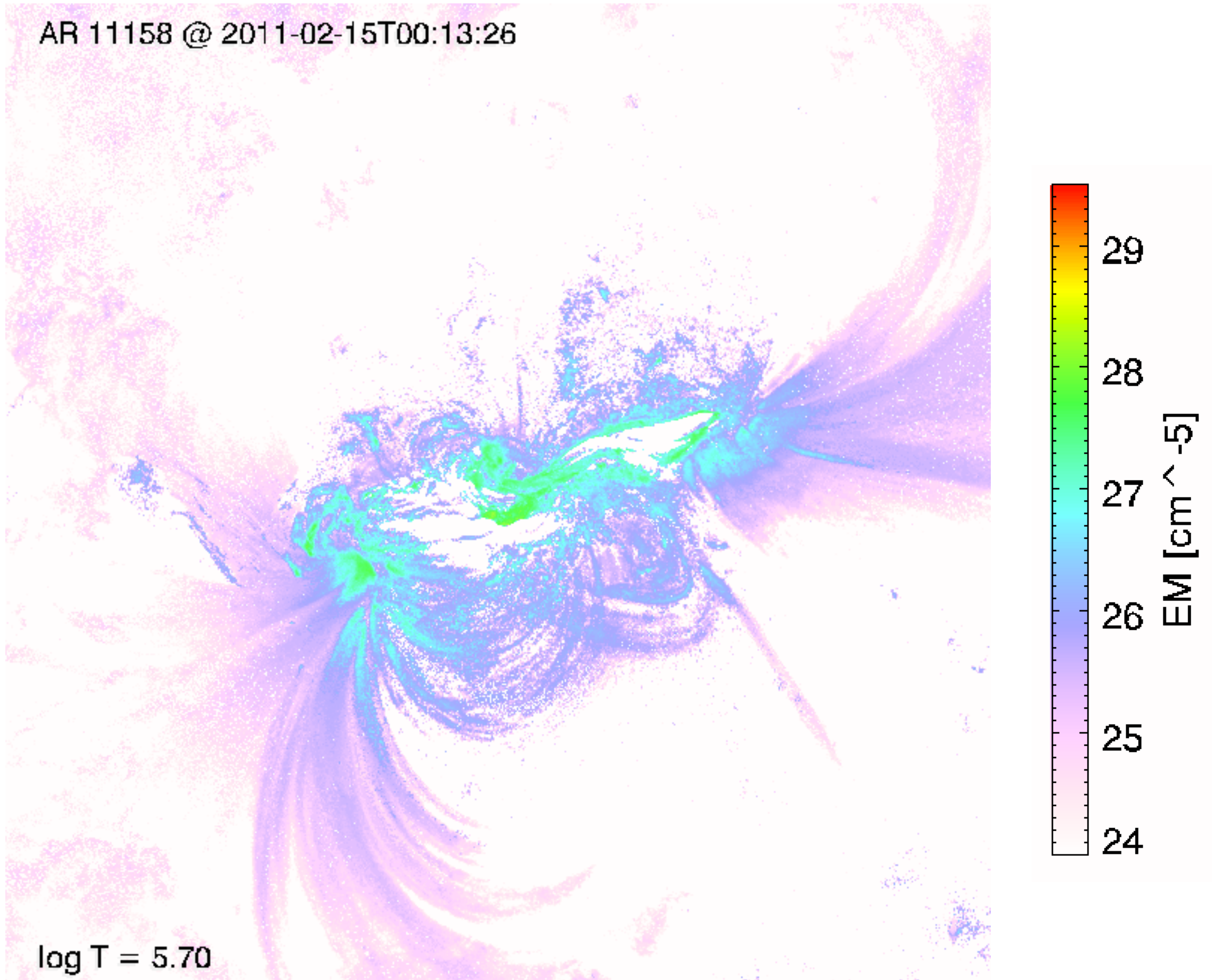

AR 11158 @ 2011-02-15T00:13:26
log T = 5.70
29
28
27
26
25
24
EM [cm ^ -5]

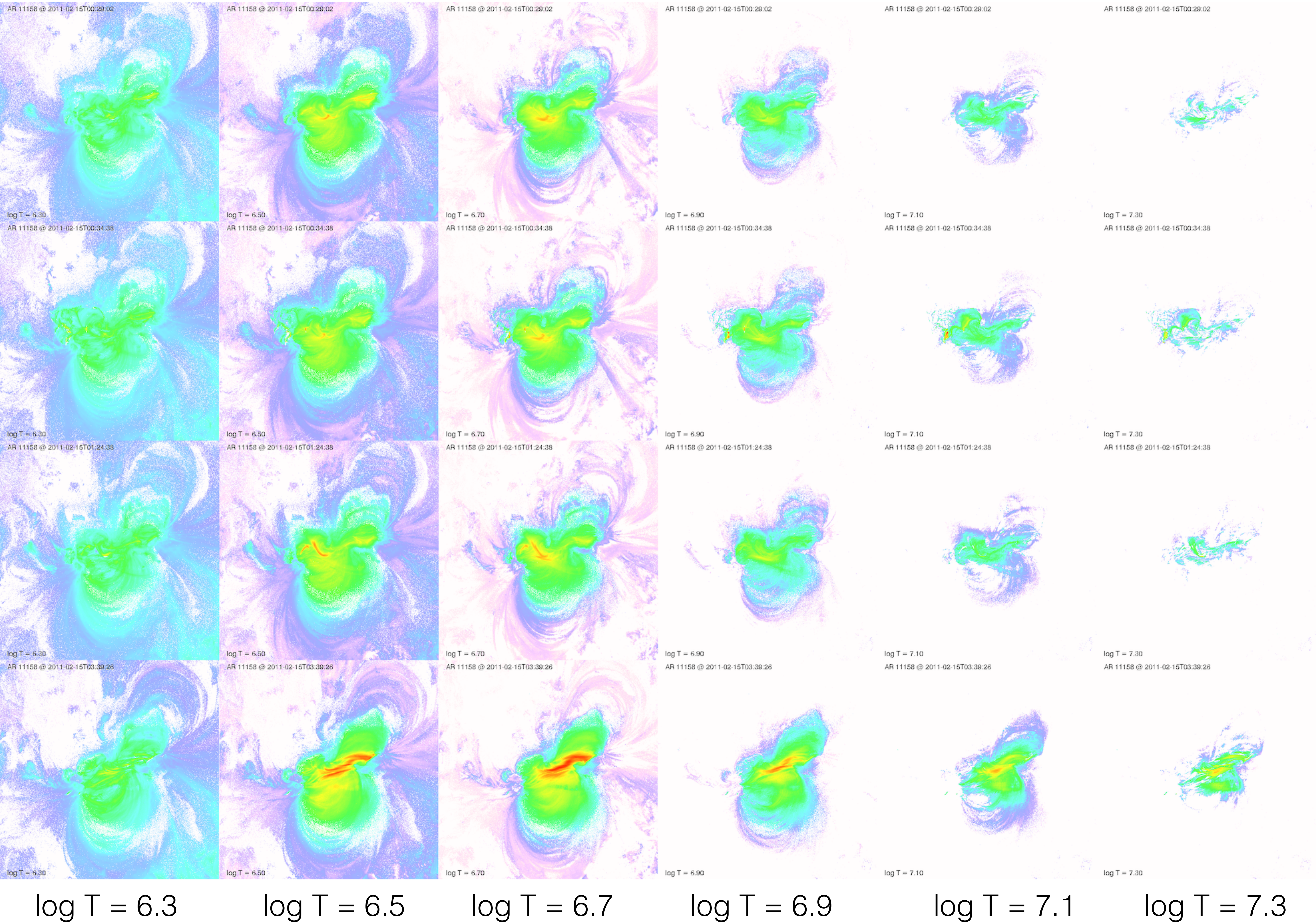
log T = 6.3
log T = 6.5
log T = 6.7
log T = 6.9
log T = 7.1
log T = 7.3

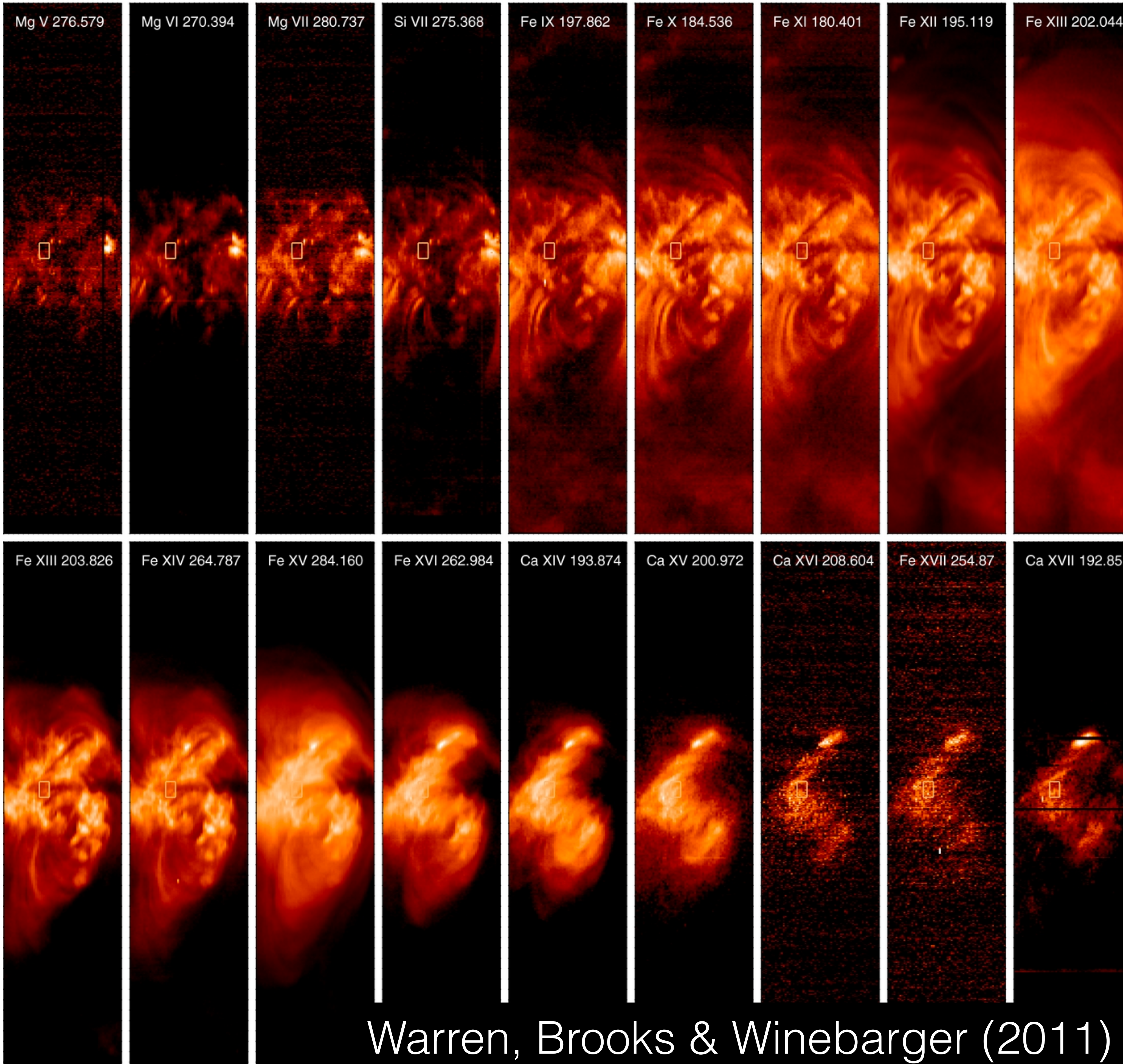

Warren, Brooks & Winebarger (2011)

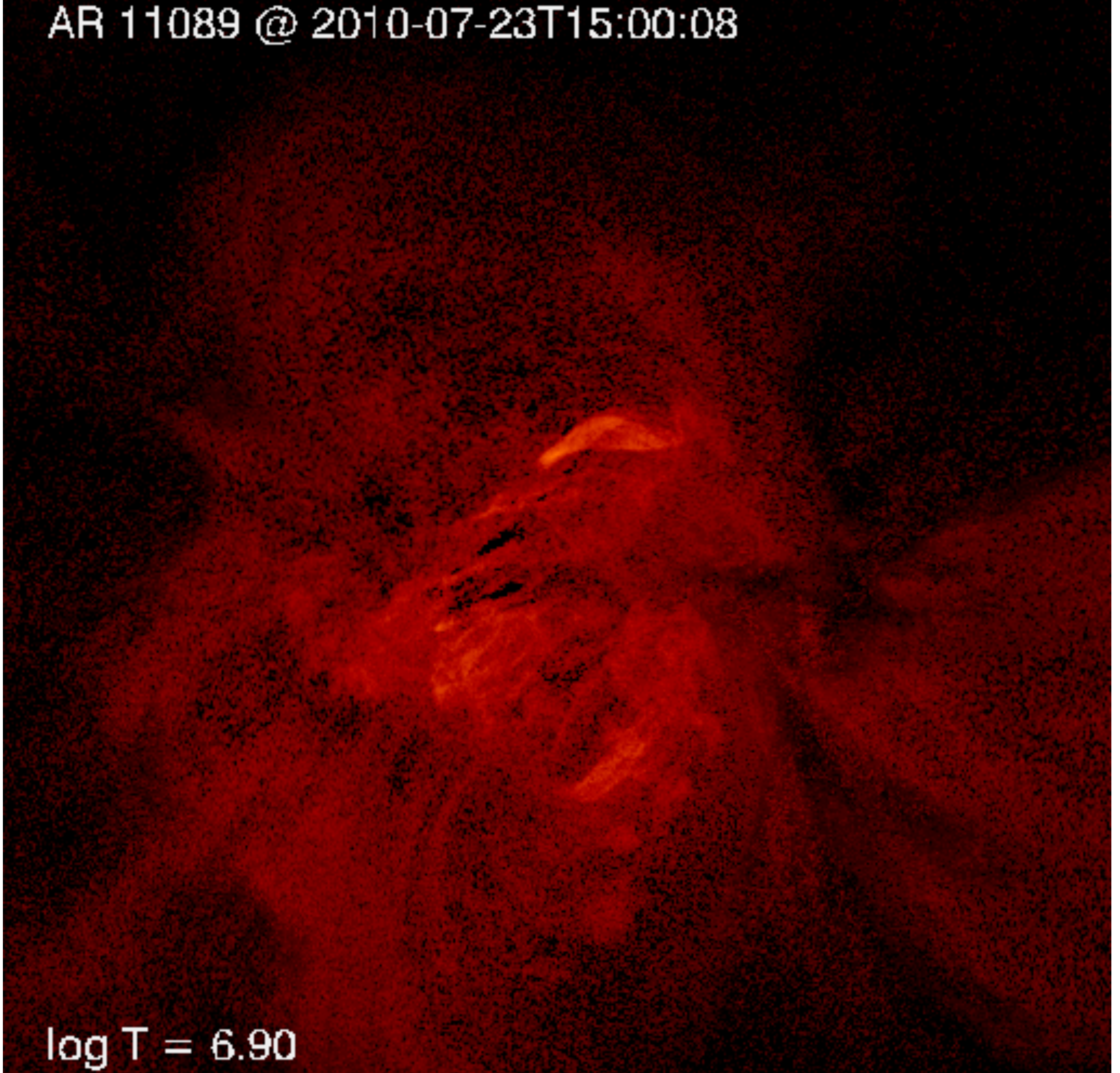
AR 11089 @ 2010-07-23T15:00:08
log T = 6.90

Side benefit: Image Denoising

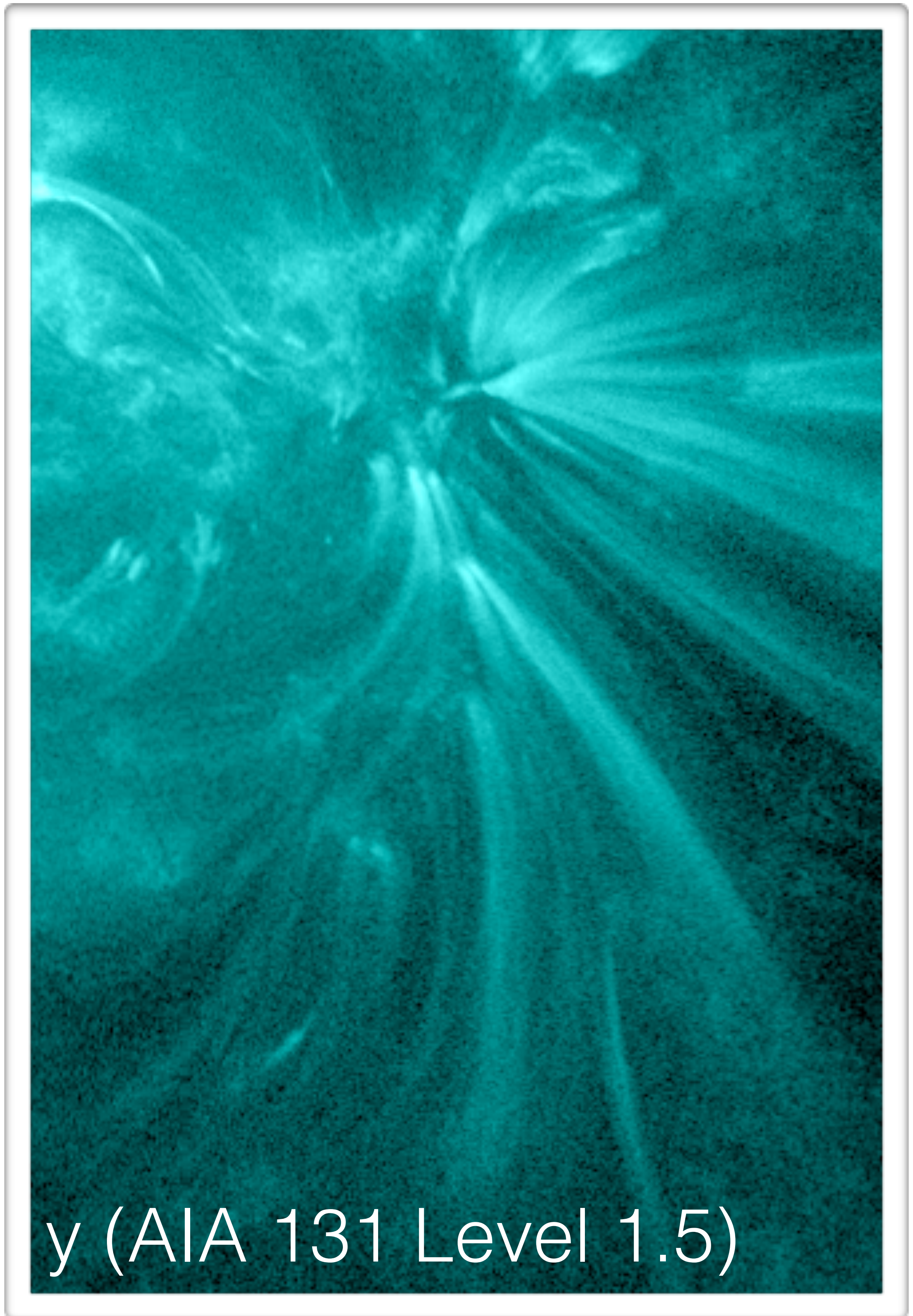

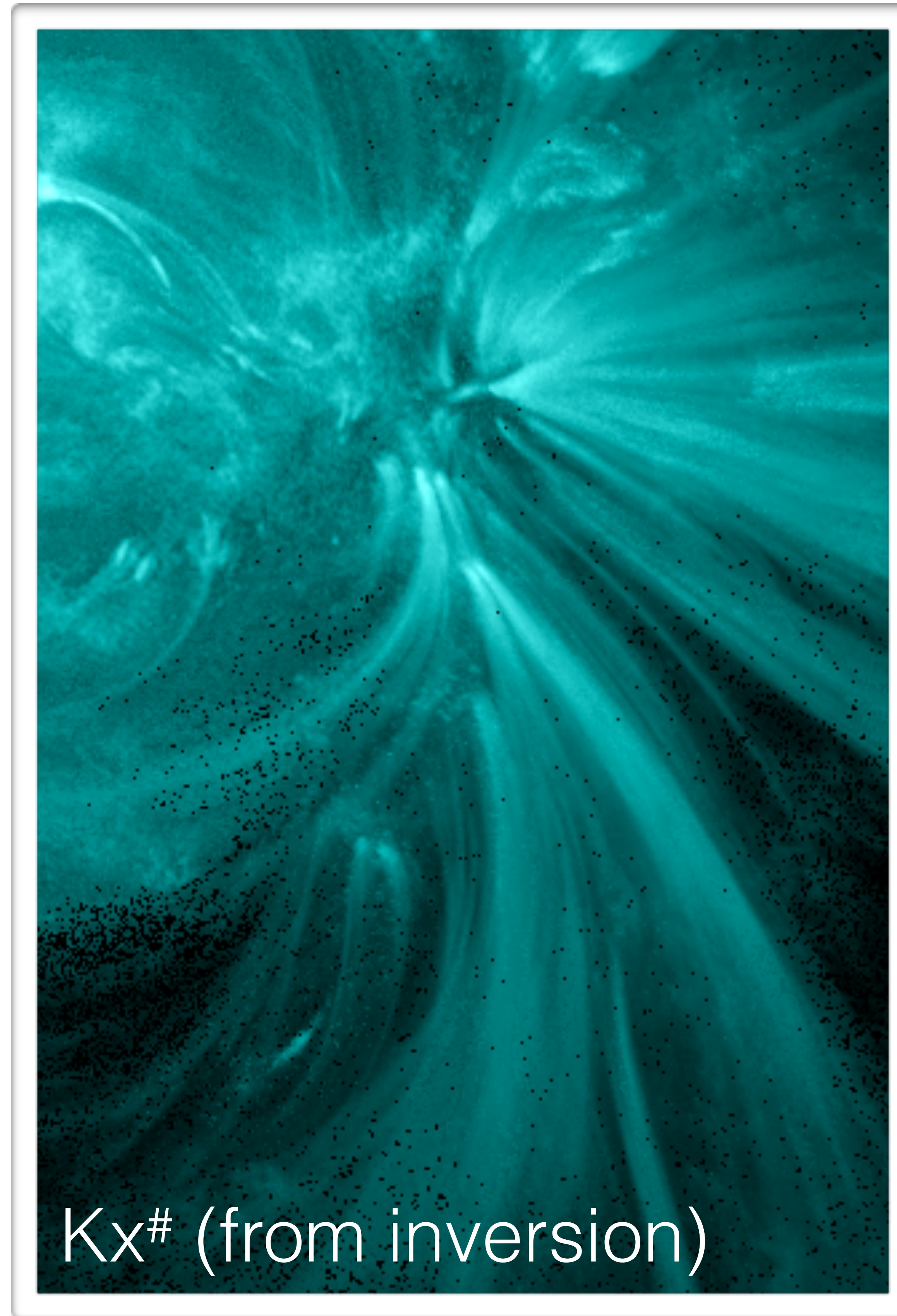

Applications

1. Evolution of Emerging Flux Regions

2. Reconnection Outflows

3. Chromospheric Evaporation and Condensation

Science Case 1) Emerging Flux

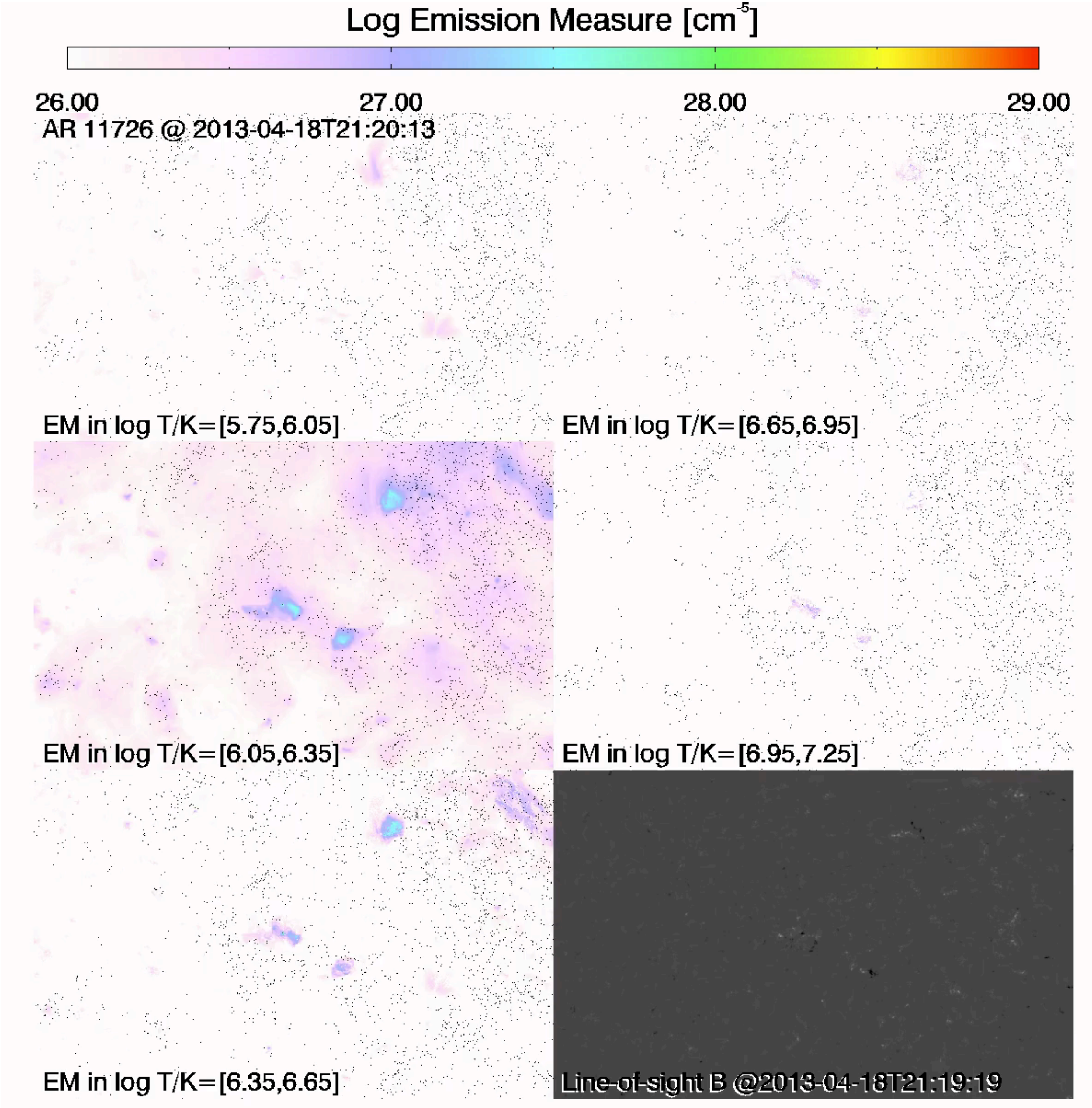

DEM movie
of the emergence
of AR 11726

Other panels:
EM in various log T bins

Lower right panel only
Greyscale:
B_{los} from HMI
Green: 6MK EM
Yellow/Red: 10 MK EM

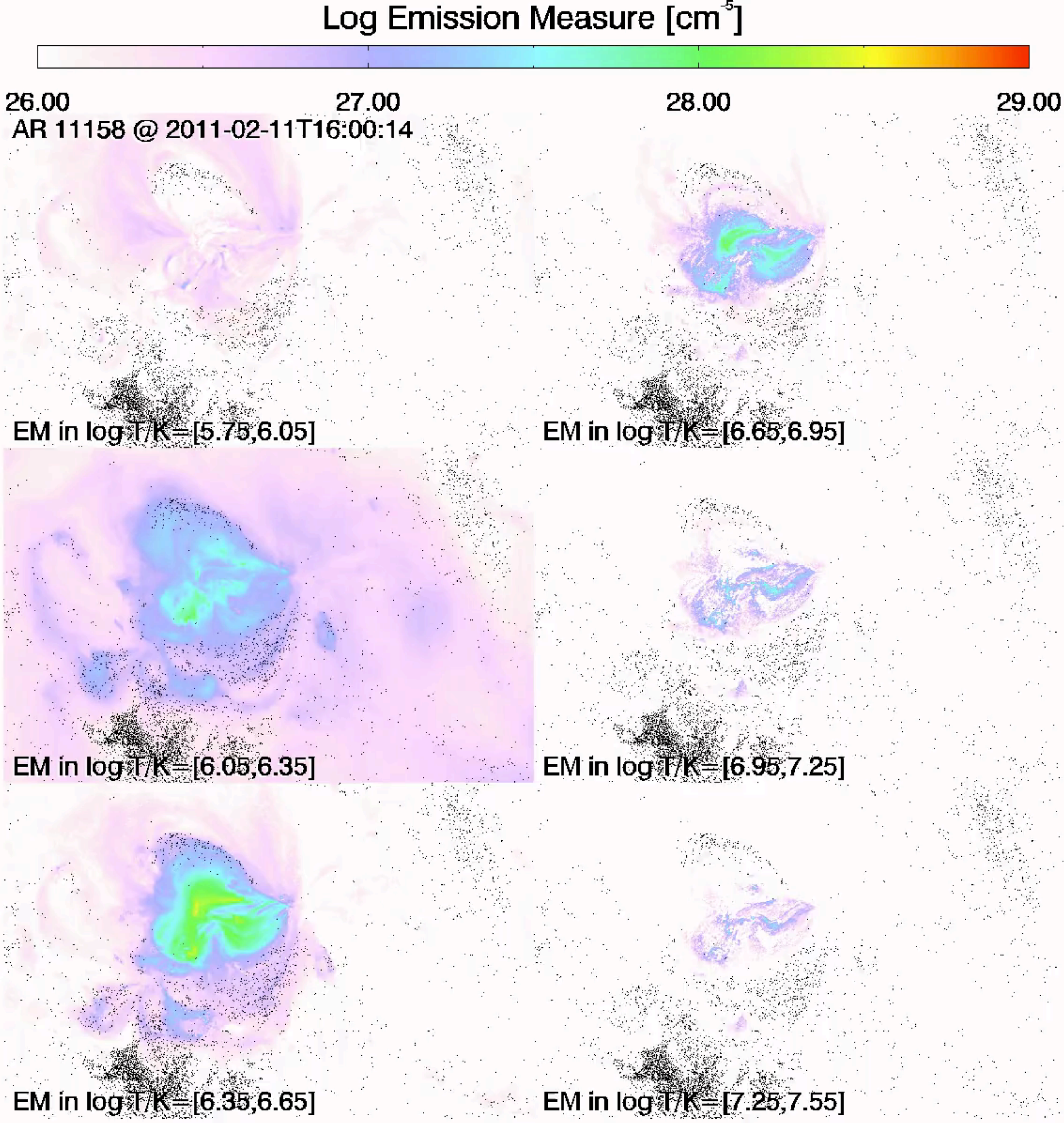

DEM movie of the emergence of AR 11158

Black pixels are where no solutions were found

Science Case 2) Reconnection Outflows

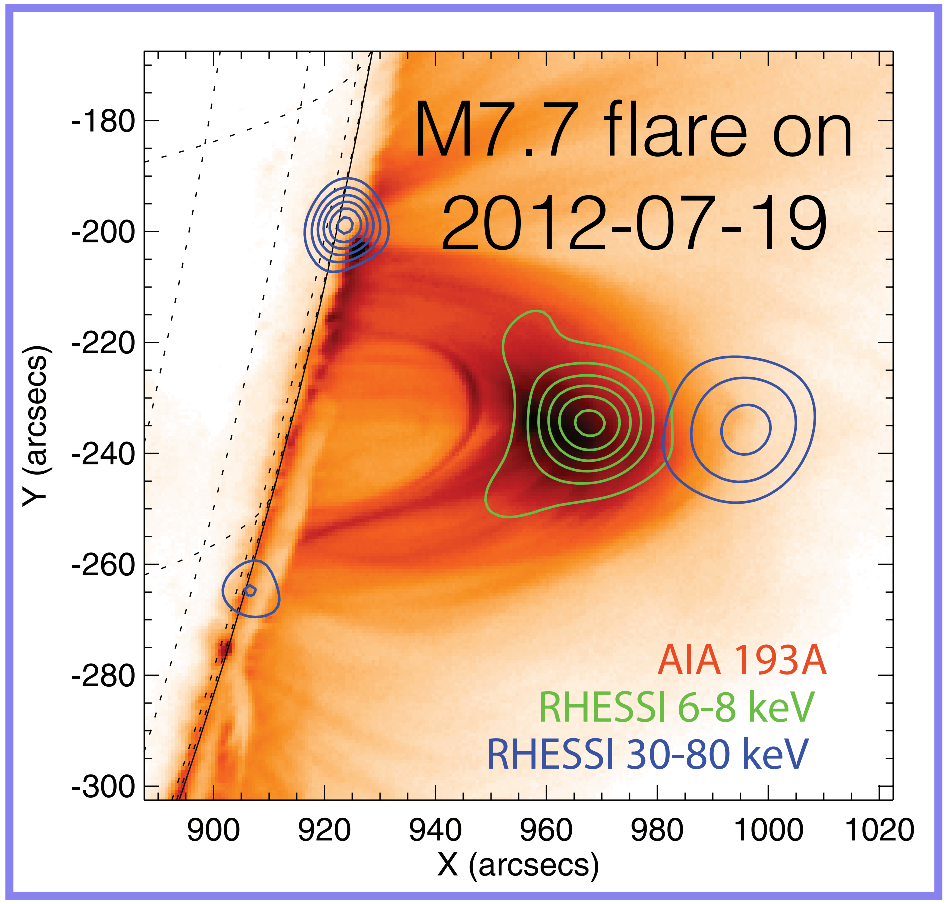

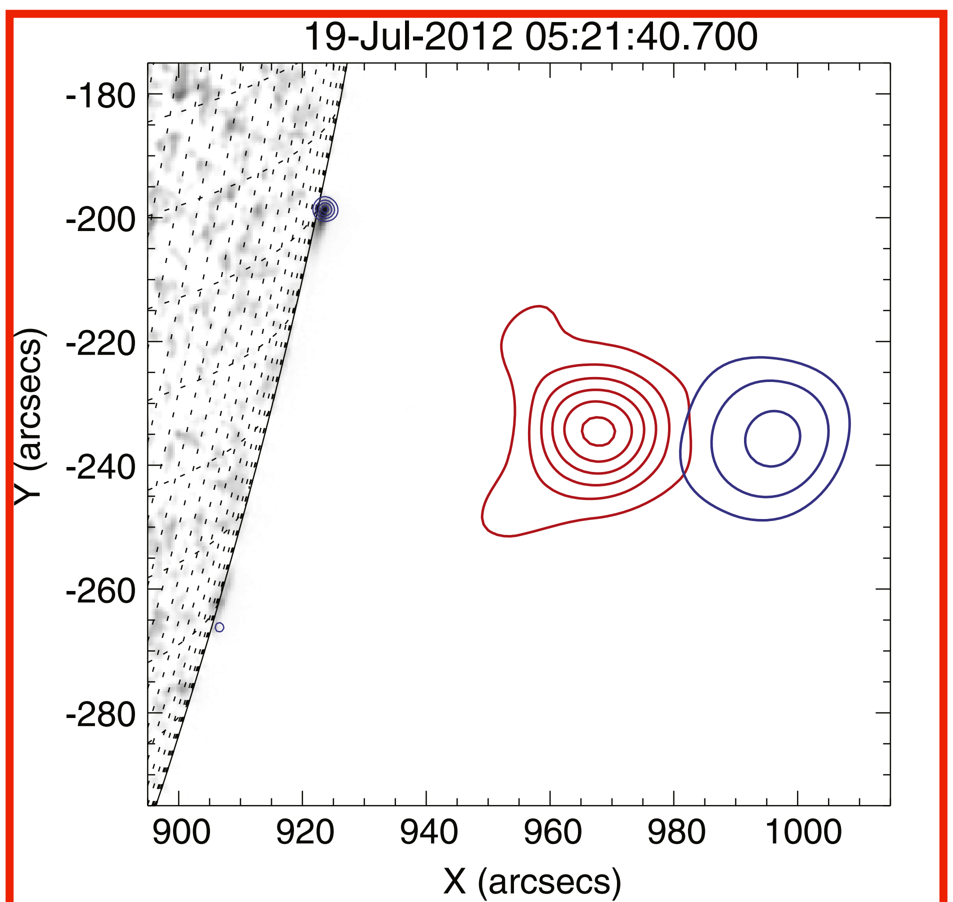

Selected scientific studies of this flare:

- Patsourakos, Vourlidas & Stenborg, 2013, ApJ, **764**, 125: **Prior confined eruption produced a pre-existing coronal flux rope, which then erupted to give the M7.7 flare.**
- Wei Liu, Chen & Petrosian, 2013, ApJ, **767**, 168: **Detailed timeline of sequence of events including timing and propagation of EUV and X-ray sources.**
- Rui Liu, 2013, MNRAS, **434**, 1309: **Same onset time for HXR and microwave (Nobeyama RH data) bursts.**
- Krücker & Battaglia , 2014, ApJ, **780**, 107: **Ratio of thermal protons (from AIA) to non-thermal electrons (from RHESSI HXR) in loop-top source is of order 1.**
- Sun, Cheng & Ding, 2014, ApJ, **786**, 73: **Performed a very detailed DEM (imaging) analysis of this flare. They used xrt_iterative_dem2.pro (code by M. Weber, non-linear least square inversion with splines).**
- Krücker et al., 2015, ApJ, **802**, 19: **HMI white light (WL) enhancement at footprint co-incident with HXR footpoint source. Interpretation: energy deposition by non-thermal electrons is radiated away and does not cause chromospheric evaporation.**

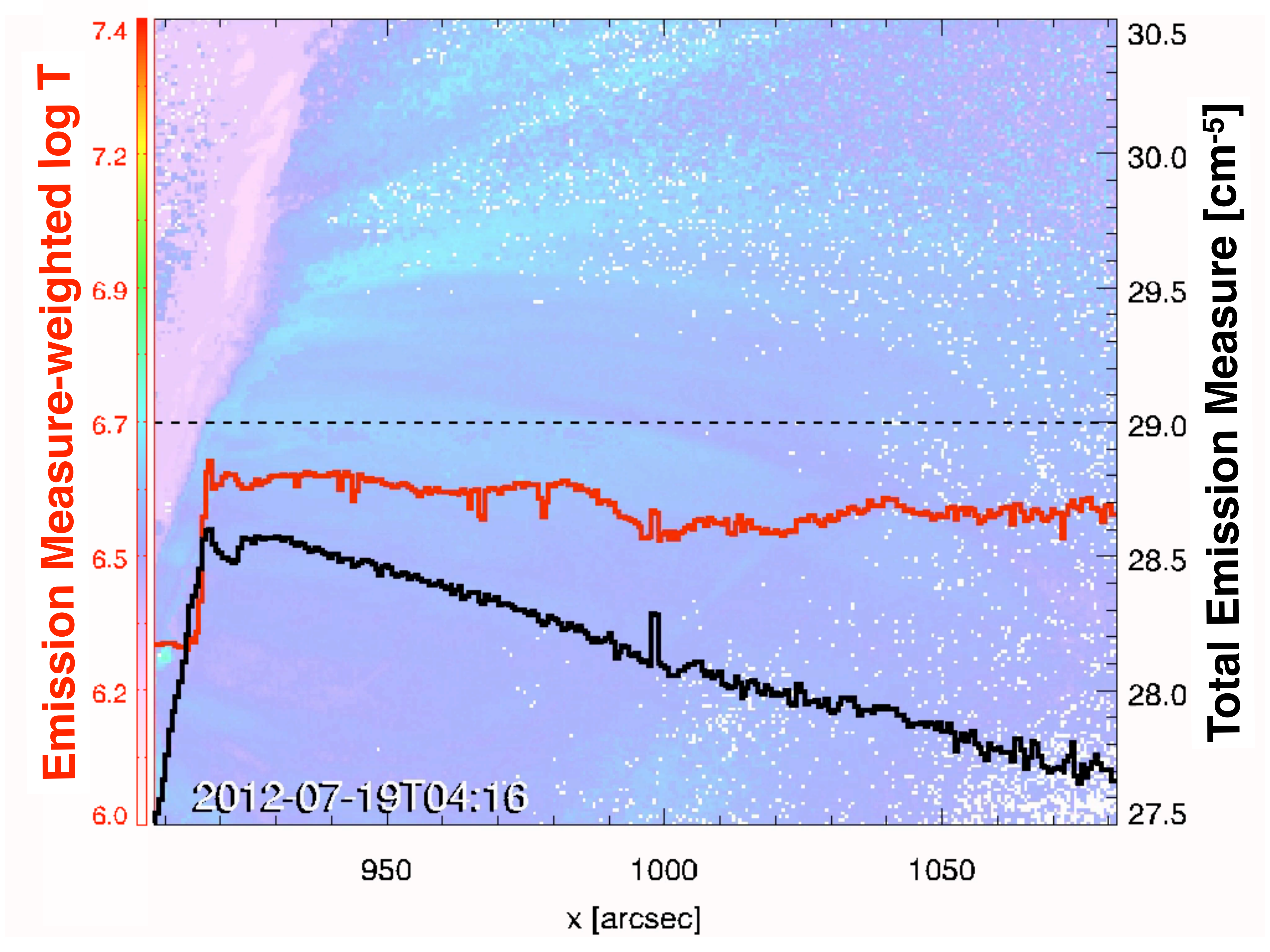
Emission Measure-weighted log T
7.4
7.2
6.9
6.7
6.5
6.2
6.0
Total Emission Measure [cm-5]
30.5
30.0
29.5
29.0
28.5
28.0
27.5
2012-07-19T04:16
950
1000
1050
x [arcsec]

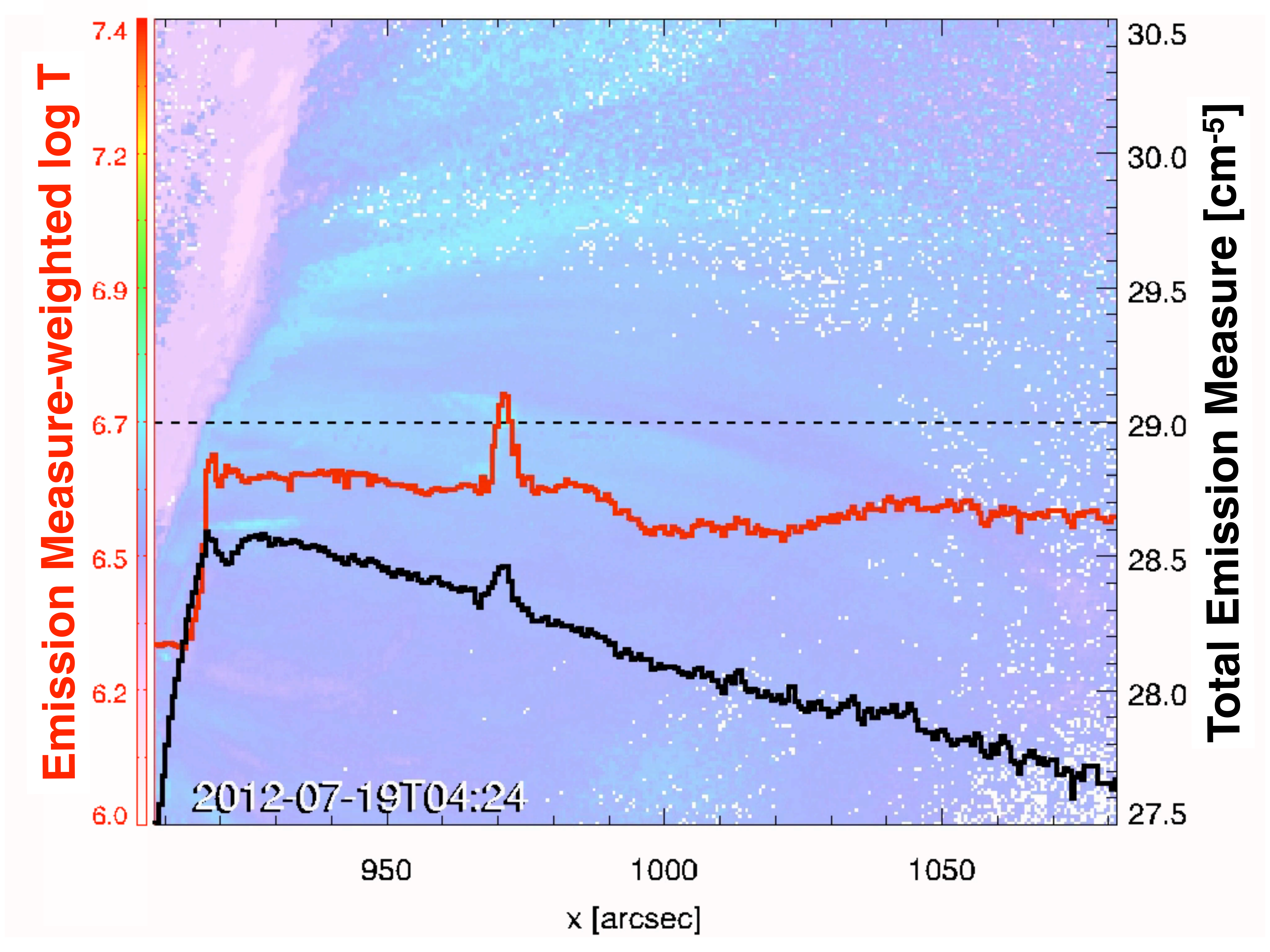

Emission Measure-weighted log T
7.4
7.2
6.9
6.7
6.5
6.2
6.0
Total Emission Measure [cm^{-5}]
30.5
30.0
29.5
29.0
28.5
28.0
27.5
2012-07-19T04:24
950
1000
1050
x [arcsec]

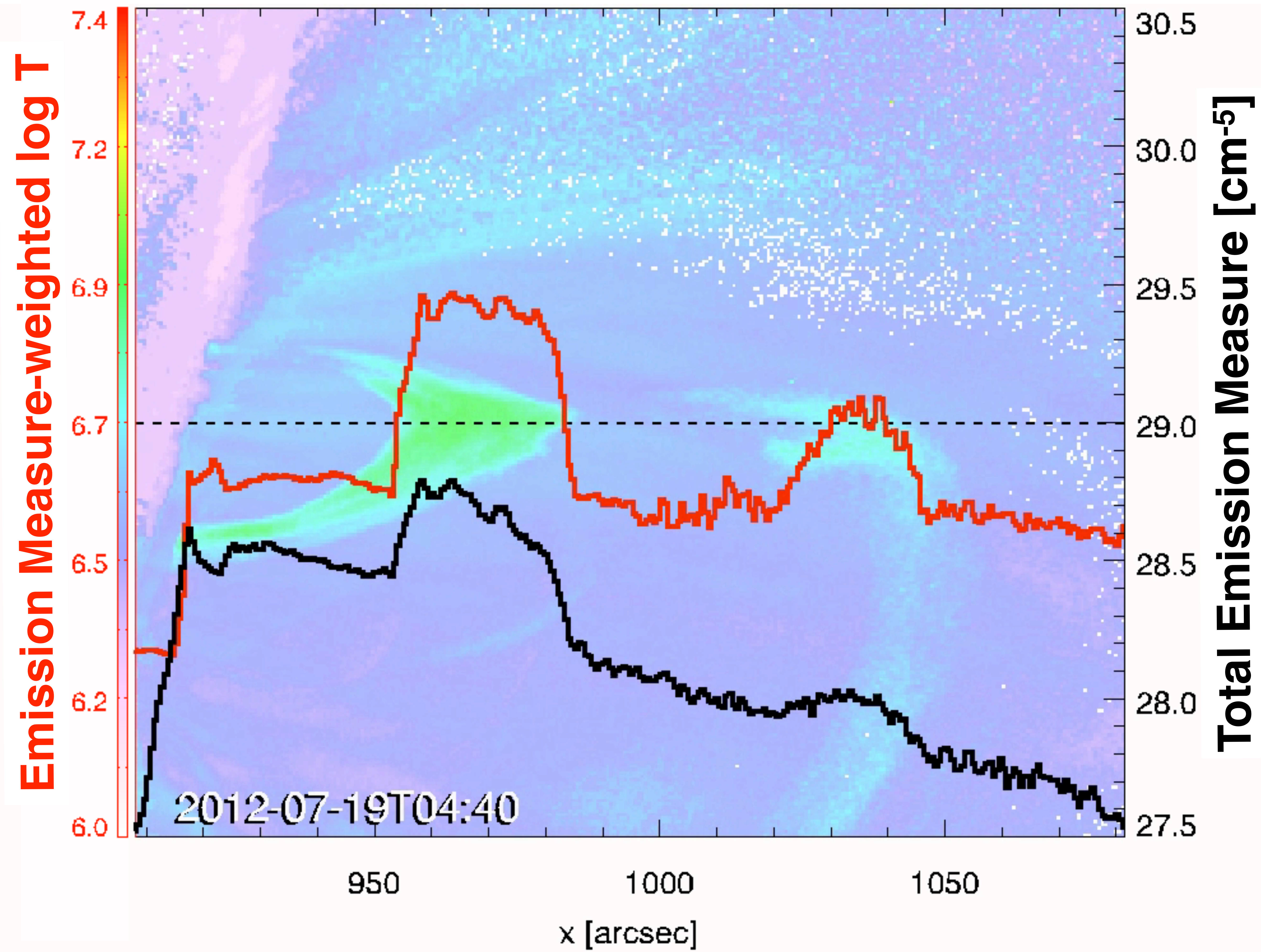

Emission Measure-weighted log T
7.4
7.2
6.9
6.7
6.5
6.2
6.0
Total Emission Measure [cm-5]
30.5
30.0
29.5
29.0
28.5
28.0
27.5
2012-07-19T04:40
950
1000
1050
x [arcsec]

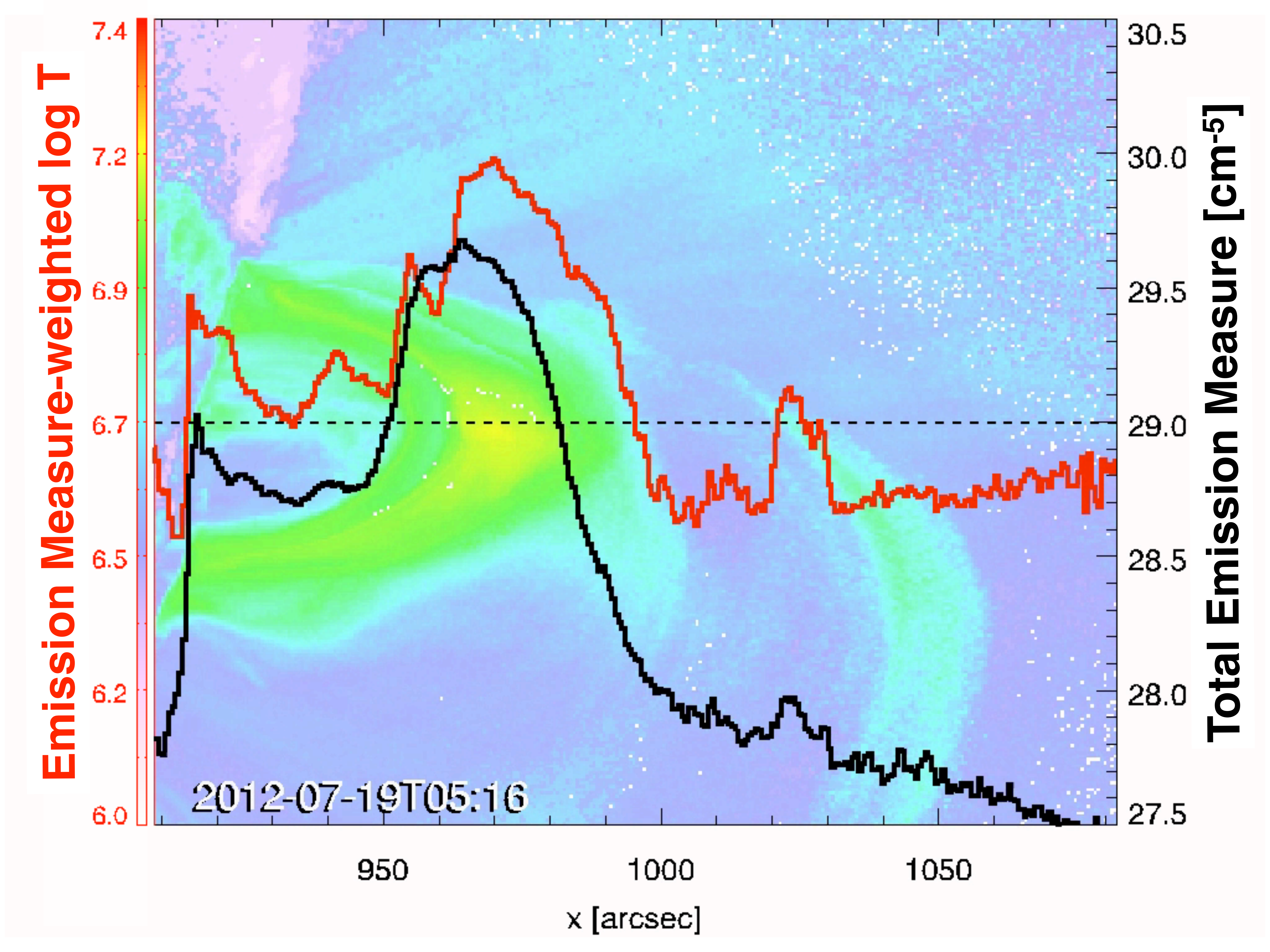
Emission Measure-weighted log T
7.4
7.2
6.9
6.7
6.5
6.2
6.0
Total Emission Measure [cm-5]
30.5
30.0
29.5
29.0
28.5
28.0
27.5
2012-07-19T05:16
950
1000
1050
x [arcsec]

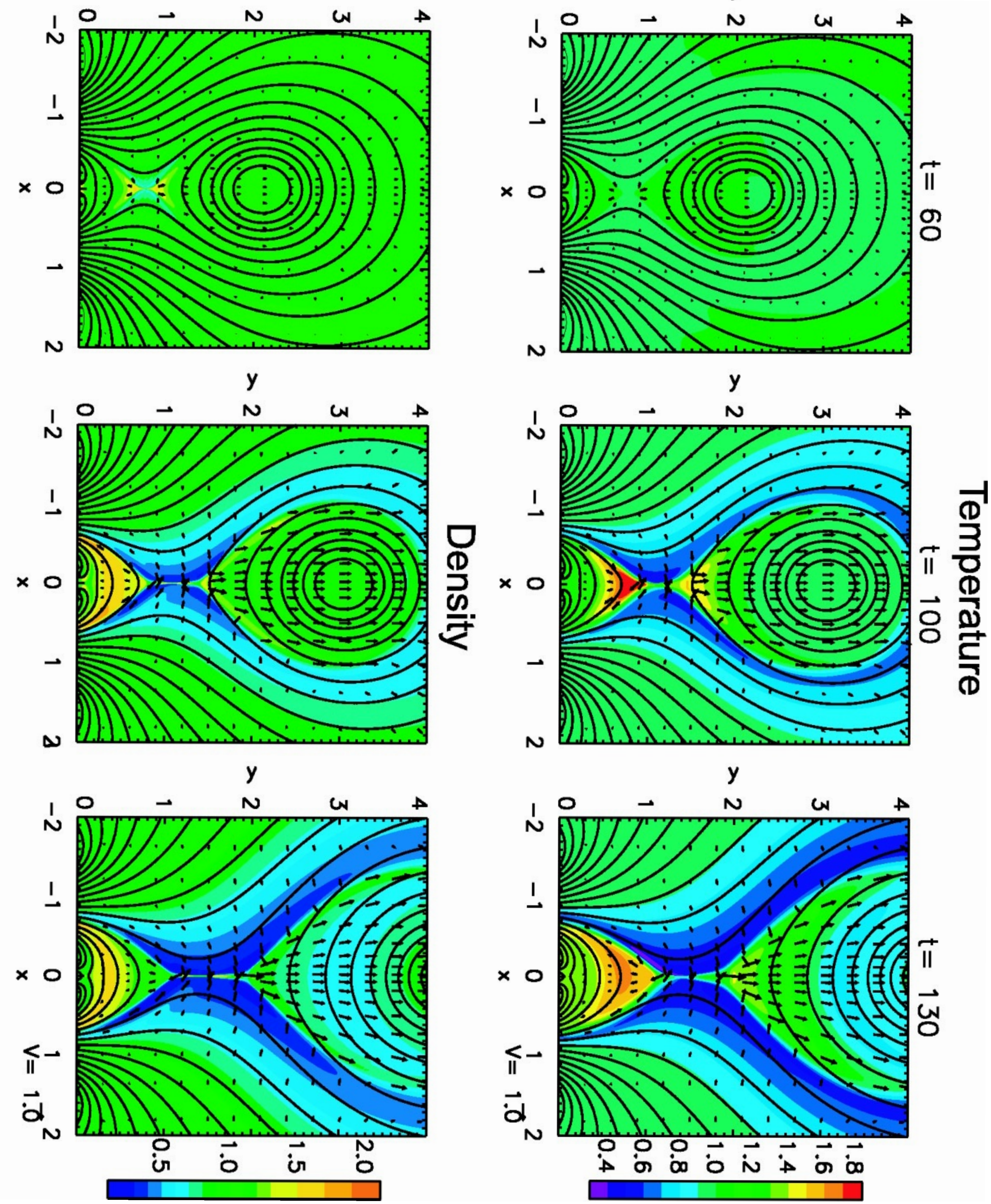

<u>Shiota et al. (2005, ApJ, **634**, 663):</u>

- 2.5D MHD simulation of of the eruption of a pre-existing flux rope triggered by flux emergence.
- Similar scenario as modeled by Chen & Shibata (2000, ApJ, **545**, 524) but with field-aligned thermal conduction.
- Both temperature and density are initially uniform (dimensionless value of unity).

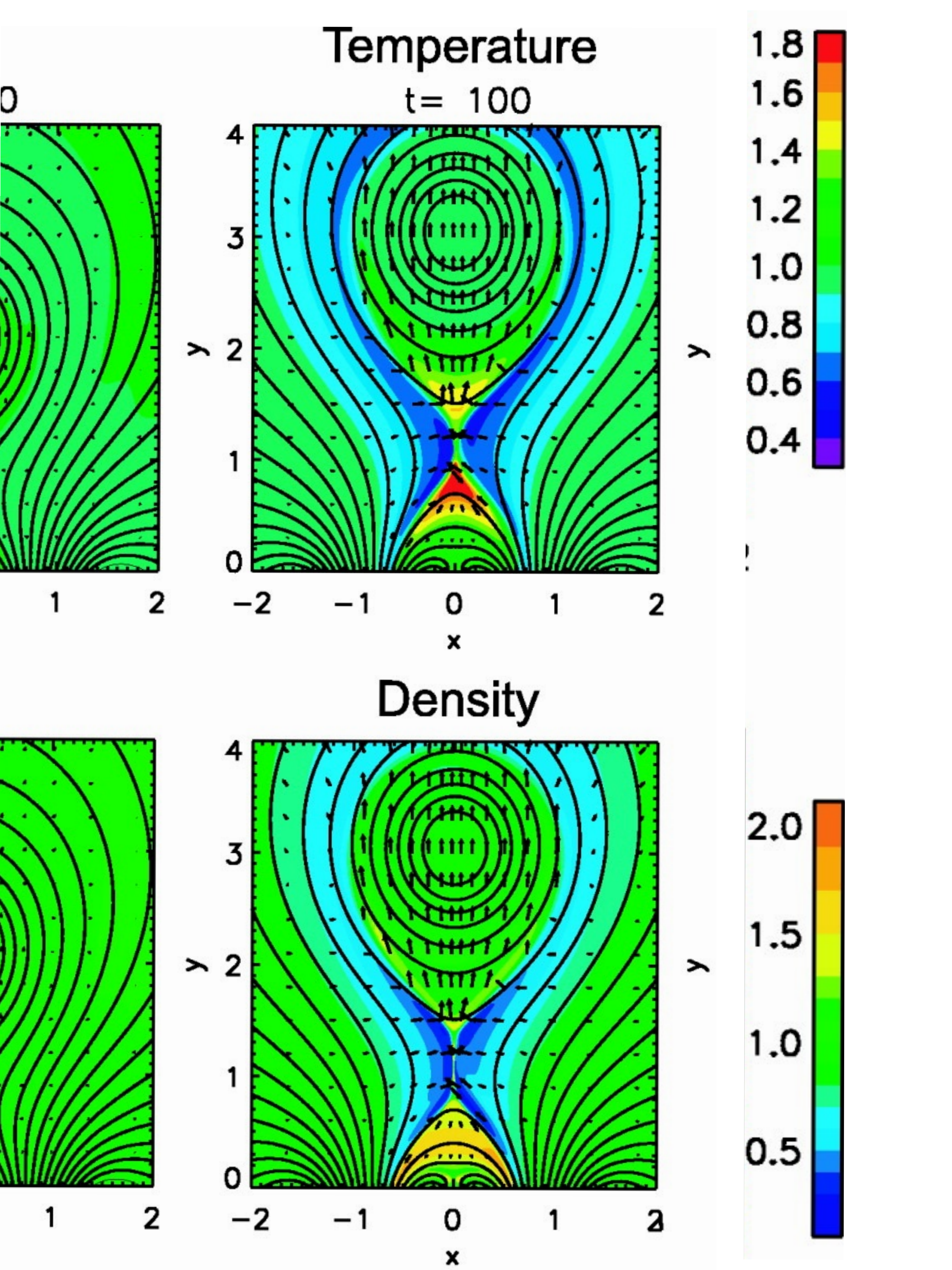

Temperature
t= 100
Density
x
y
1.8
1.6
1.4
1.2
1.0
0.8
0.6
0.4
2.0
1.5
1.0
0.5

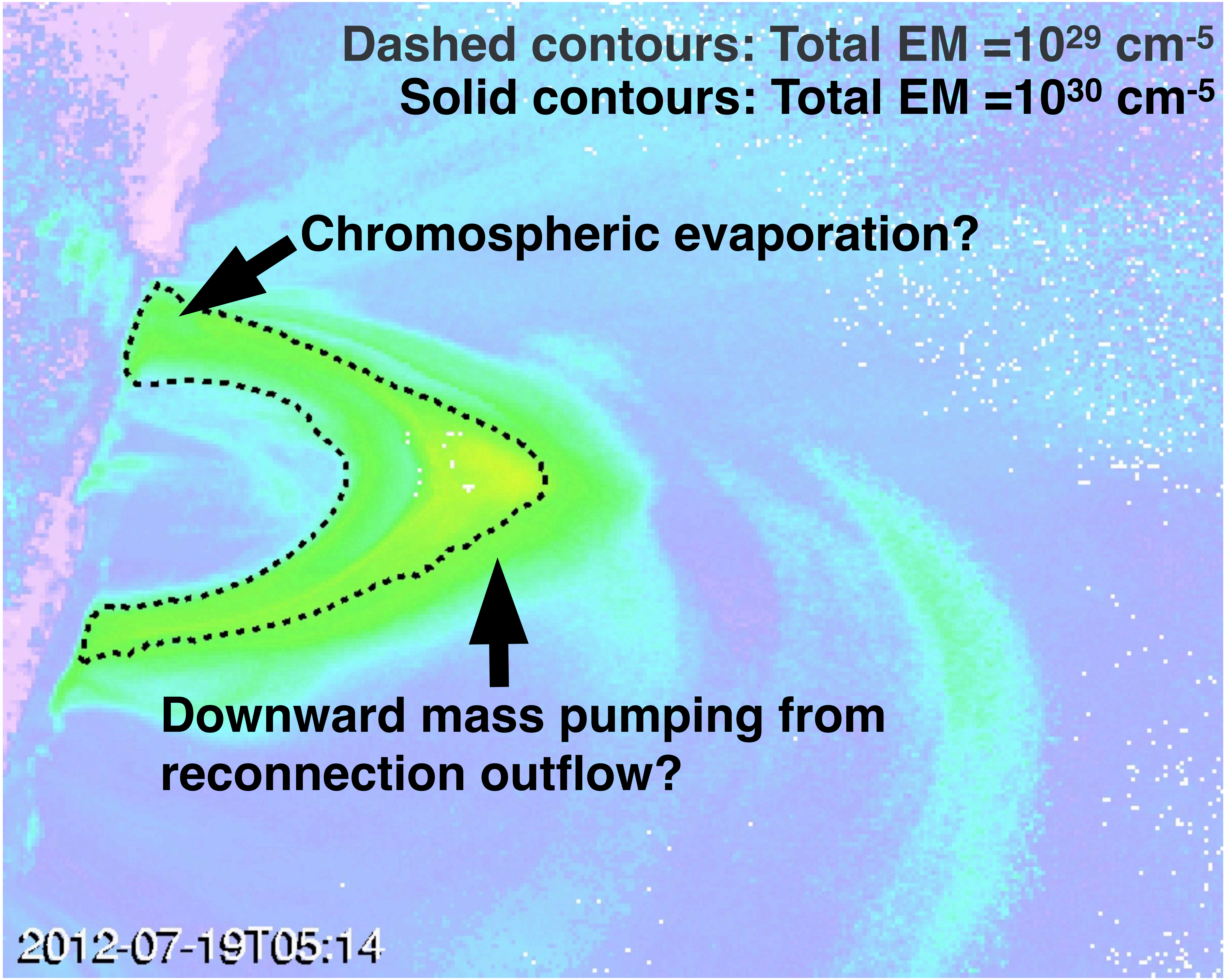
Dashed contours: Total EM =10^{29} cm^{-5}
Solid contours: Total EM =10^{30} cm^{-5}
Chromospheric evaporation?
Downward mass pumping from reconnection outflow?
2012-07-19T05:14

Science Case 3) Chromospheric Evaporation & Condensation

Observations

Spectra covering temperatures from 4,500 K to 10 MK

Images covering temperatures from 4,500 K to 65,000 K

Baseline: 5s for slit-jaw images, 1s for 6 spectral windows, rapid rastering

Predicted Count Rates

Ion Spectrum	λ	Δλ	Log T	Estimated Count Rate (counts/s/line/spatial pixel)			Detector
	Å	mÅ	K	Quiet Sun	Active Region	Flare	
UV Spectra (effective area of 2.8 cm^2 for far-UV, 0.3 cm^2 for Mg passband, continuum is 1 Å) †: Count rates for Mg II wing, h and k are in counts/s/spectral pixel/spatial pixel							
Si I (3P) Cont	1335	12.5	3.7	40	80	---	1
Mg II wing	2820	25	3.7-3.9	2100†	7500†	7500†	3
O I	1356	12.5	3.8	50	100	250	1
Mg II h	2803	25	4.0	870†	3400†	13000†	3
Mg II k	2796	25	4.0	1100†	4500†	10000†	3
C II	1335	12.5	4.3	540	1970	22000	1
C II	1336	12.5	4.3	500	1780	20000	1
Si IV	1403	12.5	4.8	400	1000	1e6	2
Si IV	1394	12.5	4.8	640	2200	3e6	2
O IV	1401	12.5	5.2	65	116	2e5	2
O IV	1400	12.5	5.2	25	60	1e5	2
Fe XII	1349	12.5	6.2	30	50	500	1
Fe XXI	1354	12.5	7.0	10	40	4e4	1
UV Slit-Jaw Images				**Estimated Count Rate (counts/s/pixel)**			
Effective area 0.005 cm^2 with 4 Å FWHM filter for Mg II; 0.7 cm^2 with 40 Å FWHM for far-UV.							
Mg II wing	2831		3.7-3.9	2300	5300	5300	4
Mg II k	2796		4.0	750	3500	8500	4
C II	1335		4.3	400	1300	13000	4
Si IV	1400		4.8	300	1200	2e5	4

From the IRIS poster @ iris.lmsal.com

IRIS is designed to probe the chromosphere and transition region, but it also sees flare plasma (Fe XXI @10 MK).

What about the temperature range in between?

Joint observations between IRIS andAIA to fill the temperature gap.

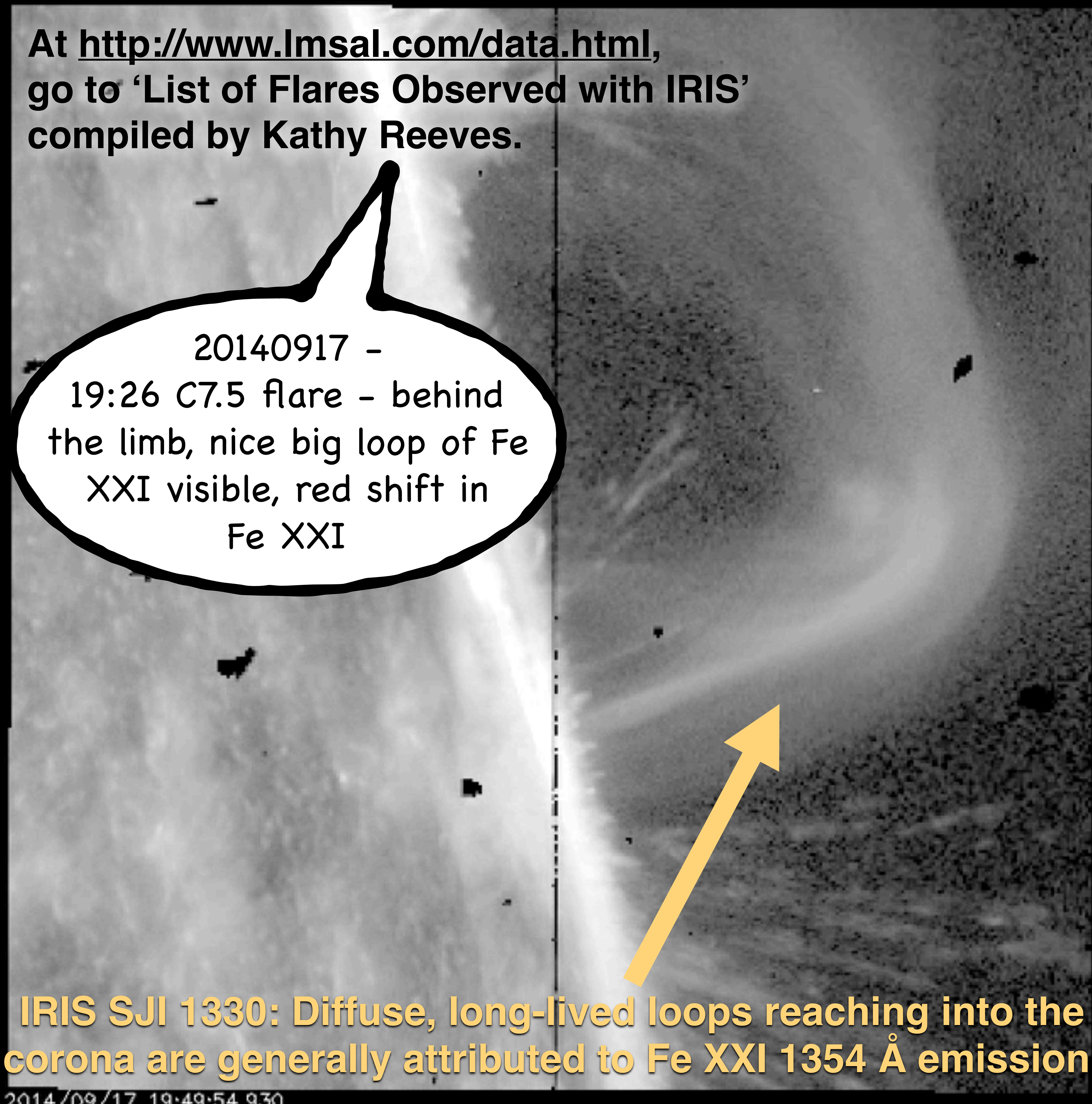
At http://www.lmsal.com/data.html,
go to 'List of Flares Observed with IRIS'
compiled by Kathy Reeves.
20140917 -
19:26 C7.5 flare - behind the limb, nice big loop of Fe XXI visible, red shift in Fe XXI
IRIS SJI 1330: Diffuse, long-lived loops reaching into the corona are generally attributed to Fe XXI 1354 Å emission.
2014/09/17 19:49:54.930

IRIS SJI 1330: Likely Fe XXI 1354 Å emission.

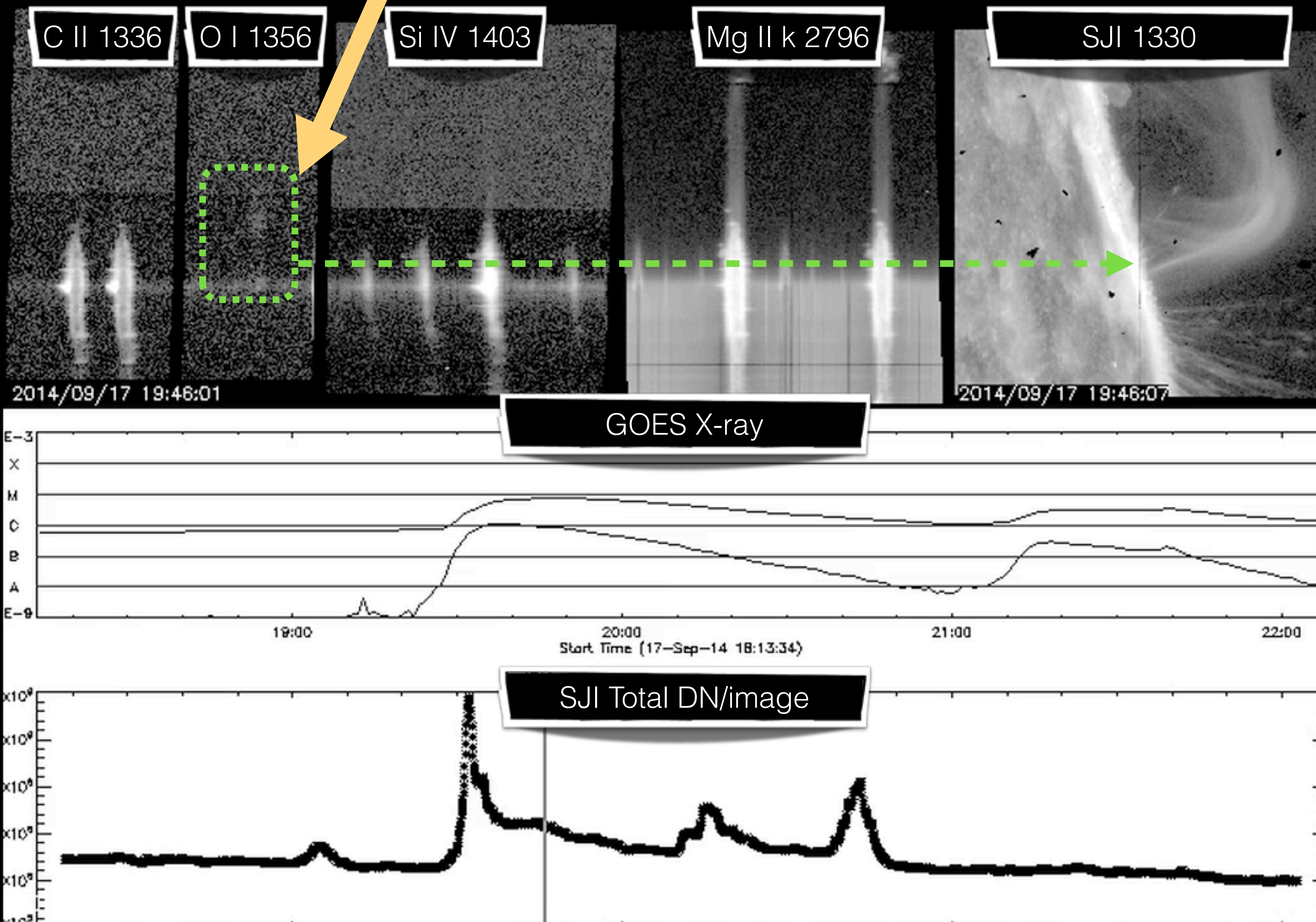

IRIS SJI 1330: Likely Fe XXI 1354 Å emission.

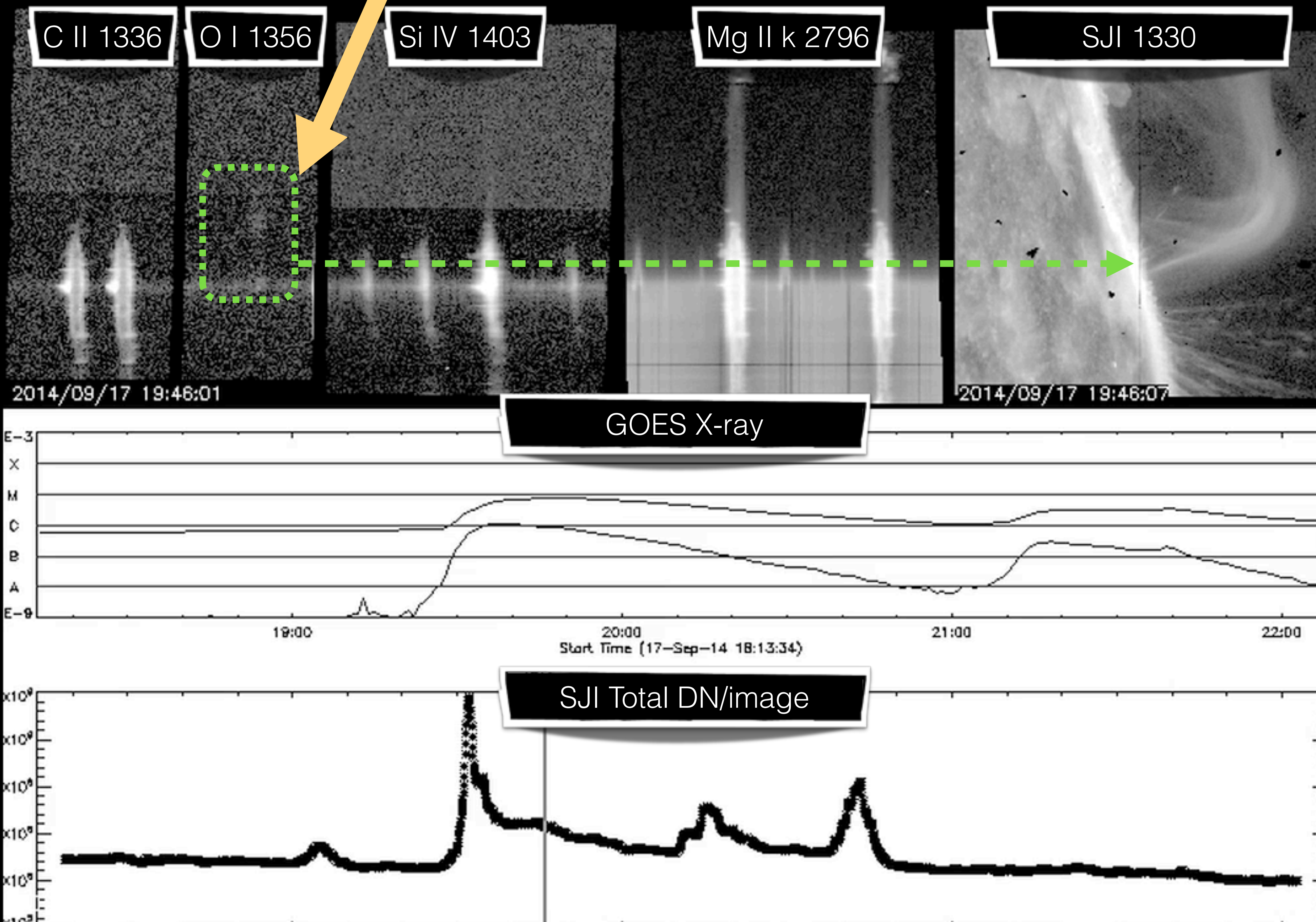

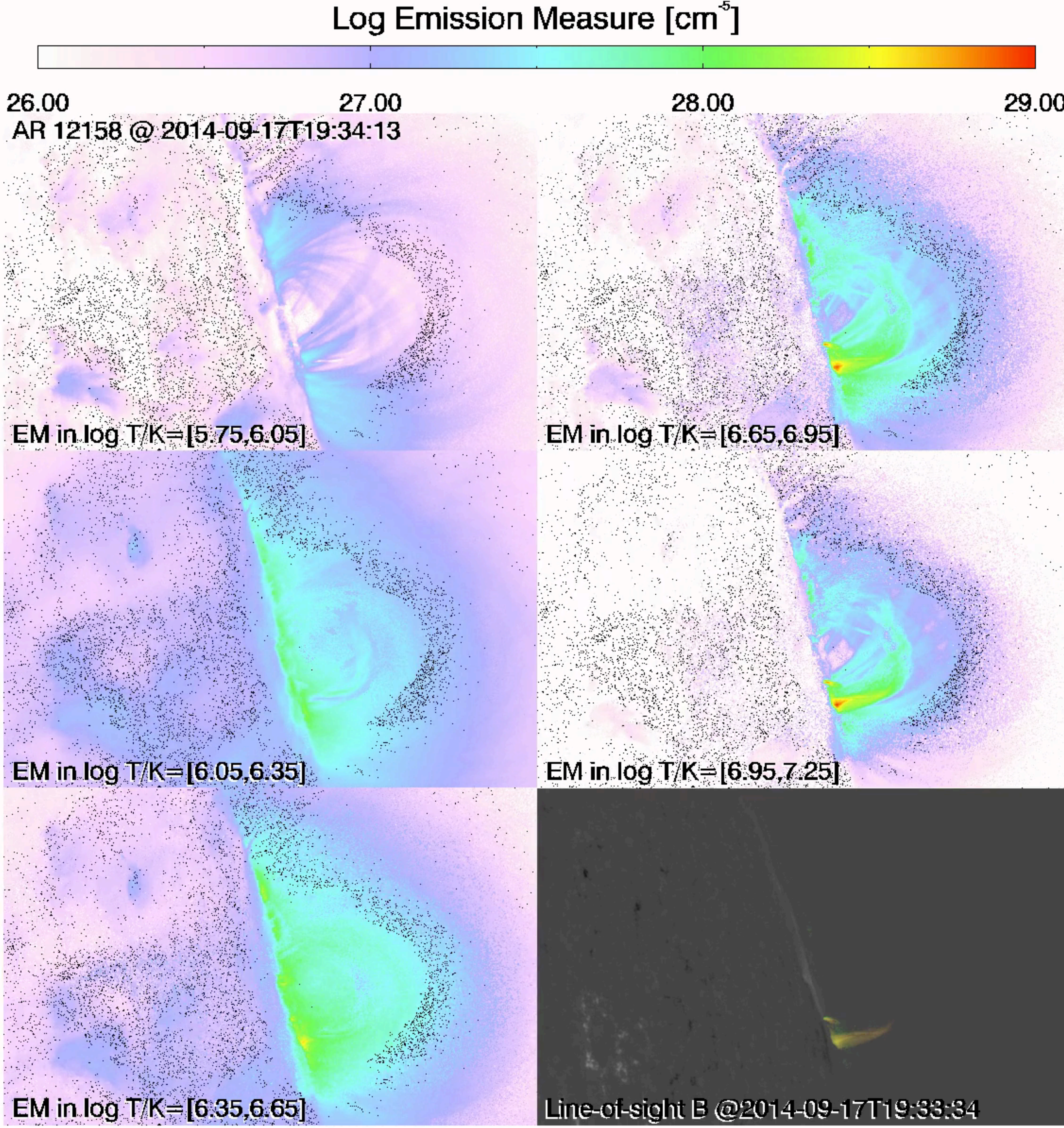

Other panels:
EM in various log T bins

- **Tell-tale signs of chromospheric evaporation**
- **Loops filled with plasma at 10 MK and above**
- **Loops cool to lower log T bins**
- **At time (~20:29 UT) when plasma cools down to log T/K ~ 5.8, coronal condensations in SJI 1330 begin to appear.**

Lower right panel only
Greyscale:
B_{los} from HMI
Green: 6MK EM
Yellow/Red: 10 MK EM

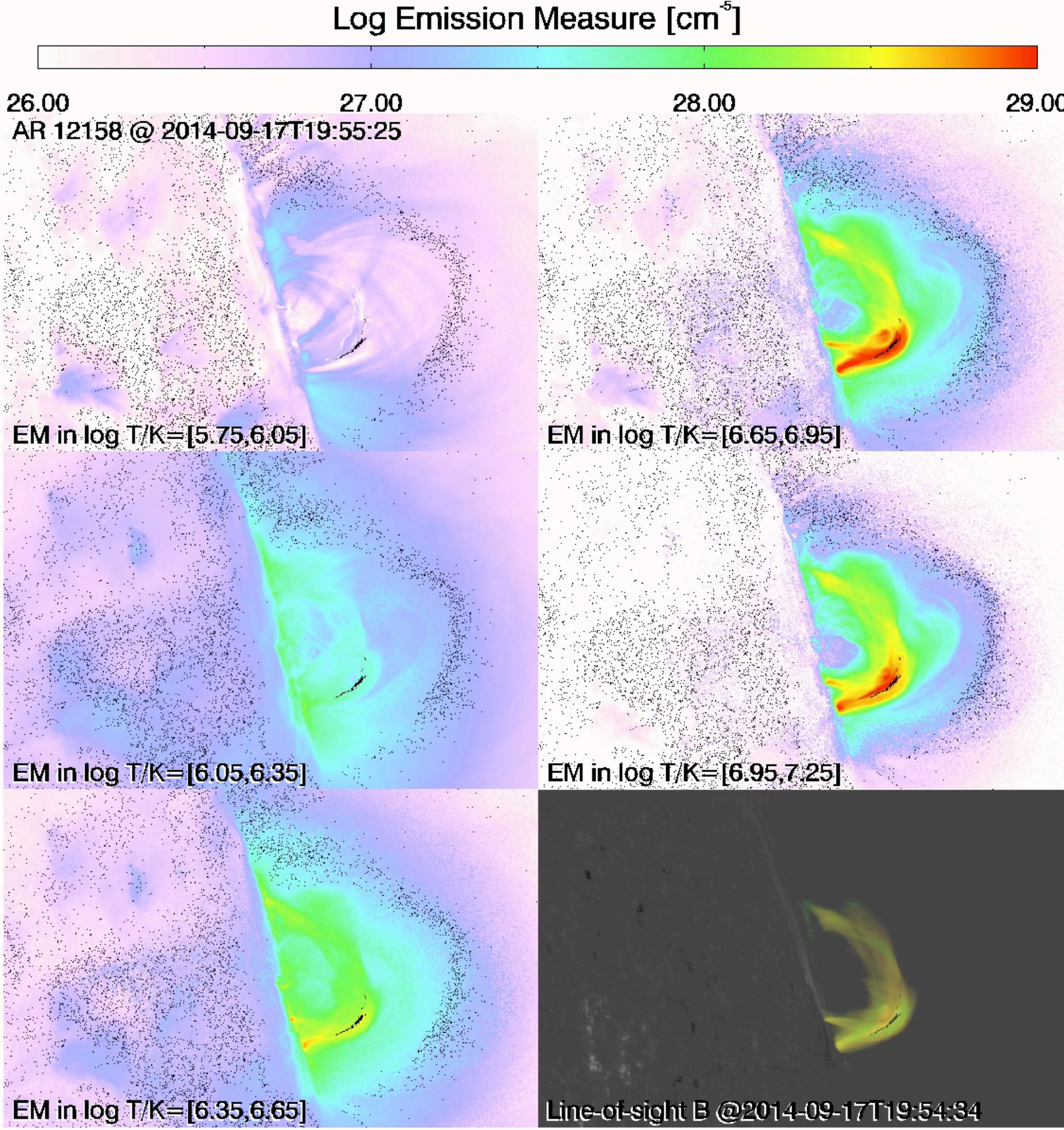

Other panels:

EM in various log T bins

- **Tell-tale signs of chromospheric evaporation**
- **Loops filled with plasma at 10 MK and above**
- **Loops cool to lower log T bins**
- **At time (~20:29 UT) when plasma cools down to log T/K ~ 5.8, coronal condensations in SJI 1330 begin to appear.**

Lower right panel only

Greyscale:

B_{los} from HMI

Yellow/Green: 6MK EM

Red: 10 MK EM

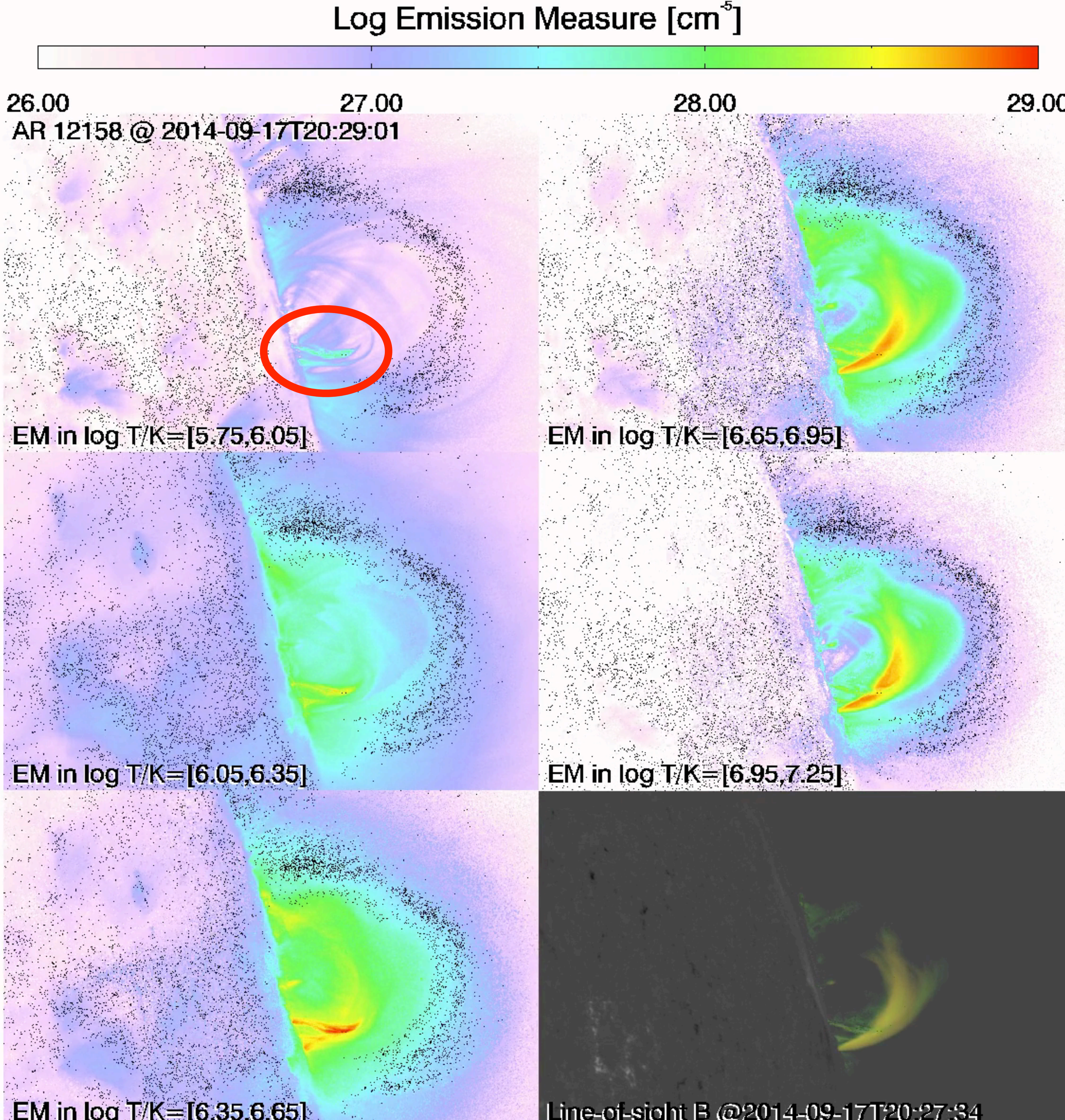

Other panels:
EM in various log T bins

- **Tell-tale signs of chromospheric evaporation**
- **Loops filled with plasma at 10 MK and above**
- **Loops cool to lower log T bins**
- **At time (~20:29 UT) when plasma cools down to log T/K ~ 5.8, coronal condensations in SJI 1330 begin to appear.**

Lower right panel only
Greyscale:
B_{los} from HMI
Yellow/Green: 6MK EM
Red: 10 MK EM

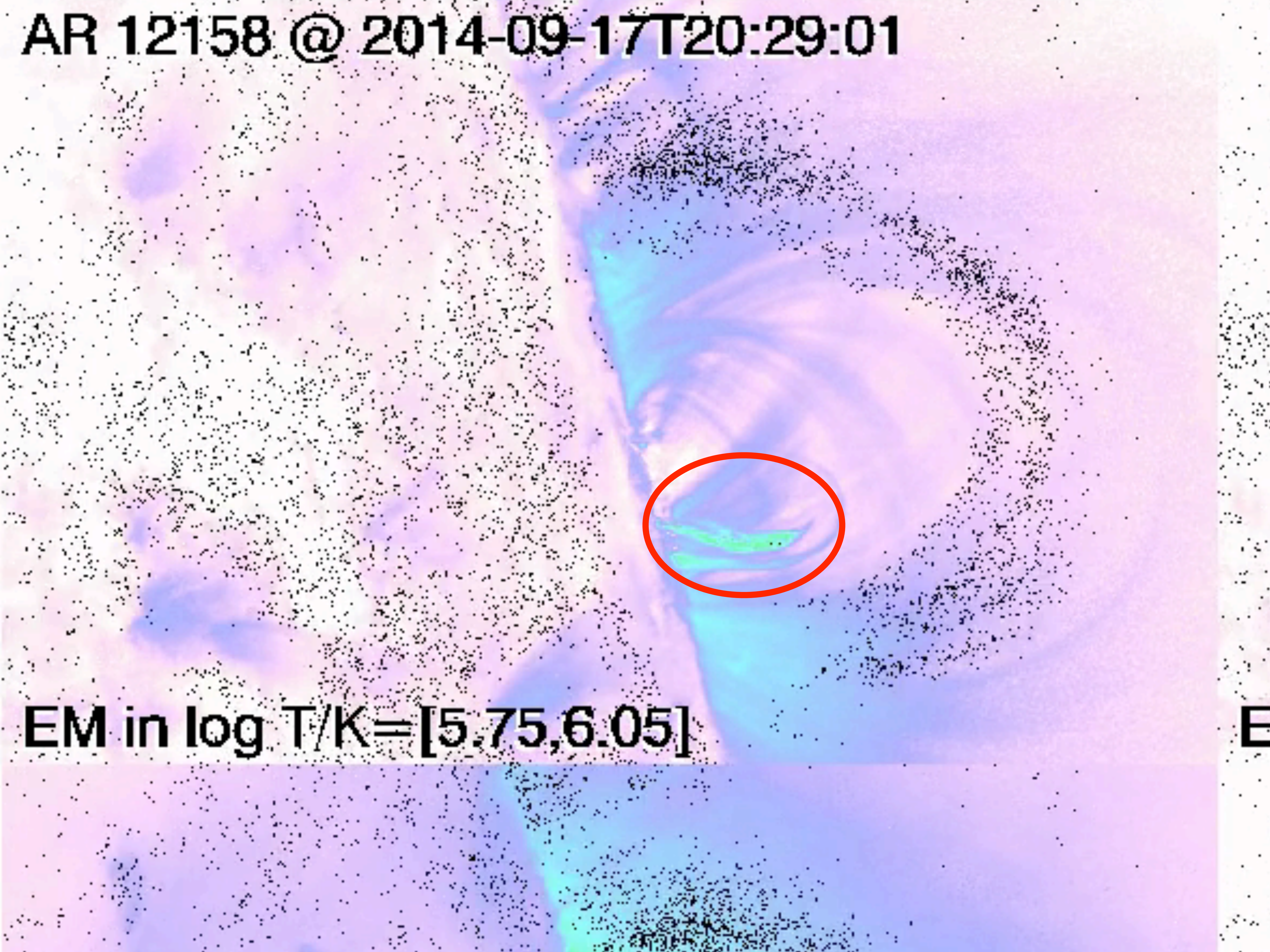
AR 12158 @ 2014-09-17T20:29:01
EM in log T/K=[5.75,6.05]

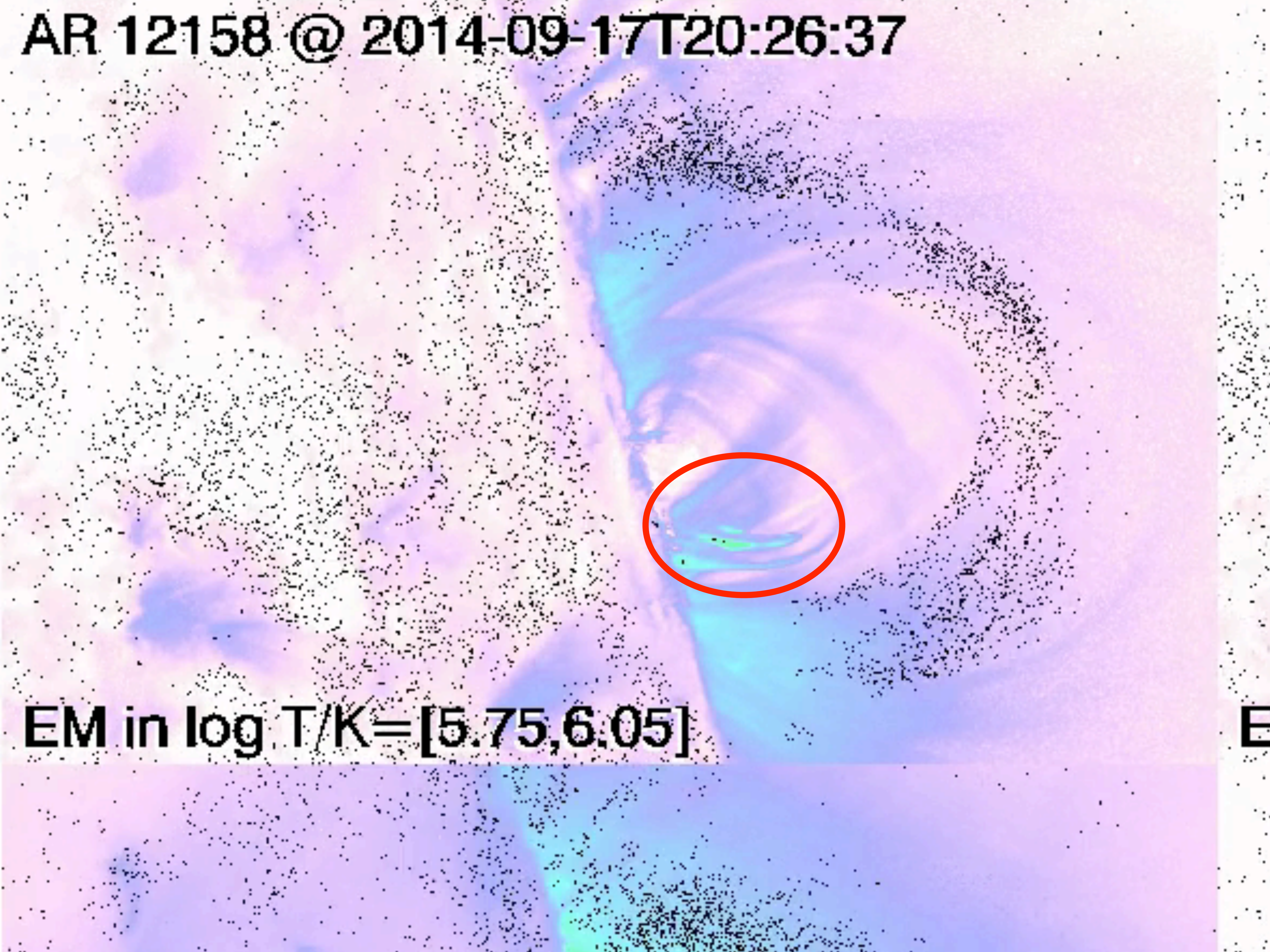
AR 12158 @ 2014-09-17T20:26:37
EM in log T/K=[5.75,6.05]

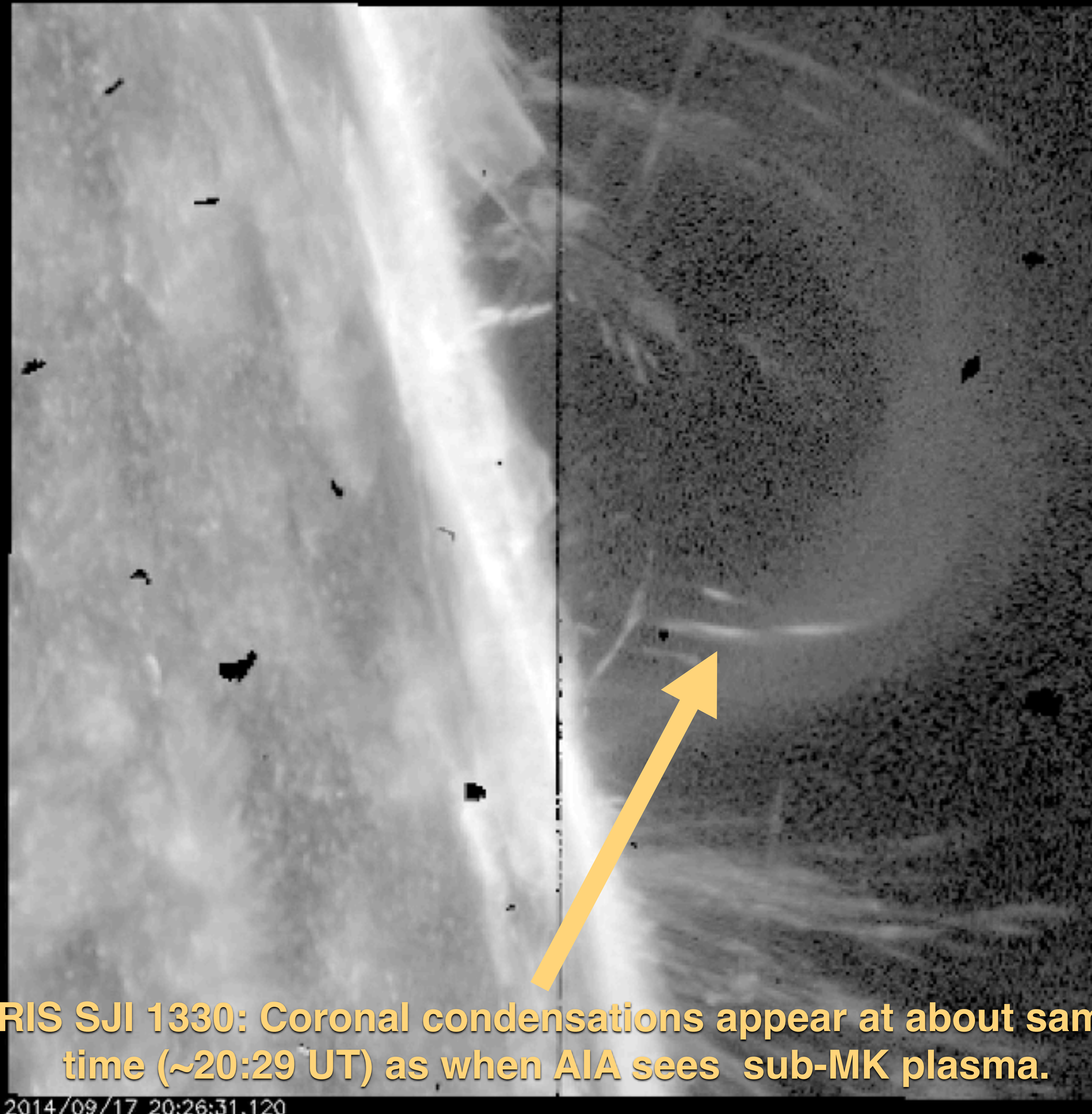

IRIS SJI 1330: Coronal condensations appear at about same time (~20:29 UT) as when AIA sees sub-MK plasma.

Summary

- Thermal diagnostics with SDO/AIA using a new, validated DEM inversion method (Cheung et al., 2015, ApJ)
  - Provides positive definite solutions.
  - Speed: O(10^4) solutions / sec with a single IDL thread.
  - Method tested against various thermal models: (1) Log-normal (Gaussian) distributions, (2) 3D models of quasi-steady loop atmospheres in a non-linear force-free field reconstruction of AR 11158, (3) MHD simulation of AR corona formation and (4) AIA-XRT cross comparison.
- Science applications
  1) Emerging Flux Regions
  2) Reconnection Outflows
  3) Chromospheric Evaporation & Condensation
- AIA and IRIS together give temperature coverage from the quiet chromosphere to the flaring corona.

How to use the Sparse DEM code

http://www.lmsal.com/~cheung/AIA/tutorial_dem/

- Instructions in the readme file
- Download *genx files, which contain sample AIA 6-channel data.
- Download aia_sparse_em_init.pro & exercise1.pro

➡ .compile aia_sparse_em_init

➡ .r exercise1

Output image of exercise1.pro